Chaotic flows and fast magnetic dynamos

John M. Finn and Edward Ott[a)]
Laboratory for Plasma and Fusion Energy Studies, University of Maryland, College Park, Maryland 20742

(Received 13 January 1988; accepted 9 June 1988)

Given a prescribed flow of an initially unmagnetized conducting fluid, one can ask if a small seed magnetic field will amplify exponentially with time. This is called the kinematic dynamo problem. In many cases of interest (particularly in astrophysics), very high electrical conductivity of the fluid (high magnetic Reynolds number R_m) is relevant. In this paper the kinematic dynamo problem is considered in the $R_m \to \infty$ limit (the "fast" kinematic dynamo). It appears that an important ingredient for a kinematic dynamo in this limit is that the orbits of fluid elements in the flow be chaotic. In this paper it is shown that the magnetic field tends to concentrate on a zero volume fractal set, and, in addition, tends to exhibit arbitrarily fine-scaled oscillations between parallel and antiparallel directions. Idealized analyzable examples exhibiting these properties are presented, along with numerical computations on more typical examples. For the latter a numerical technique for treating fast dynamos is developed and its properties are discussed. The relation of the dynamo growth rate to quantitative measures of chaos, namely, the Lyapunov exponent and topological entropy, is also discussed.

I. INTRODUCTION

Magnetic fields are a pervasive phenomenon in the universe. They occur in planets (e.g., the Earth's field), in stars, in interplanetary space, as well as on galactic and intergalactic scales.[1,2] A natural approach toward explaining the observed prevalence of magnetic fields is formulated in the so-called kinematic dynamo problem[1-16]: *Given a prescribed flow of an initially unmagnetized conducting fluid, will a small seed magnetic field amplify exponentially with time*?

Since the flow is prescribed, the resulting equation for the magnetic field is linear. The solution of the kinematic dynamo problem, in general, depends on the particular flow and on the electrical resistivity of the fluid. Zeldovich and Ruzmaikin[7,11] distinguish between "fast" and "slow" dynamo flows. In a fast dynamo, γ, the exponential growth rate of the magnetic field, approaches a positive value as the resistivity approaches zero. In a slow dynamo, γ becomes negative or approaches zero as the resistivity approaches zero. This is illustrated schematically in Fig. 1, where the horizontal axis is the magnetic Reynolds number $R_m = v_0 L_0/\eta$ (here v_0 and L_0 denote characteristic velocity and length scales of the flow, η is the electrical resistivity of the fluid, and we use a system of units where the magnetic permittivity μ_0 is unity). The magnetic Reynolds number can be very large in many situations (e.g., $R_m \gtrsim 10^8$ in the sun), and it is consequently thought that only fast dynamos are of interest in such cases.

It is the purpose of this paper to investigate fast dynamos by studying the kinematic dynamo equation with zero resistivity. Since the limit $\eta \to 0$ is very singular[10] (as will become evident subsequently), it is not immediately clear how the solution of the $\eta = 0$ equation is related to the solution with a small but finite η. This question and the relevance of chaotic flows to the fast dynamo problem are discussed in Secs. II and III.

In Sec. IV we introduce a class of two-dimensional maps as a model for fast chaotic dynamo action. Using these maps we show that, as time goes on, the magnetic flux tends to become more and more spatially intermittent, eventually concentrating on a fractal set whose dimension we can calculate in terms of the map parameters. Also using these models, we show that if any cancellation of magnetic field is possible, cancellation becomes more and more prevalent as time goes on. That is, in the zero resistivity limit, the upward directed fraction of the total magnetic flux through a surface exponentially approaches the fraction that is downward through the surface. This occurs on ever finer scales as time proceeds. Thus there will be more and more rapid spatial oscillation between large upward and downward magnetic field vectors. The growth of net flux through a given surface can still occur, however, if the exponential increase of the upward and downward fluxes individually exceeds their relative exponential rate of approach toward each other. See Bayly and Childress[16] for a related discussion of the effect of cancellation on dynamo action. The tendency toward cancellation and the tendency for the fields to concentrate on a zero volume fractal set pose inherent difficulties for compu-

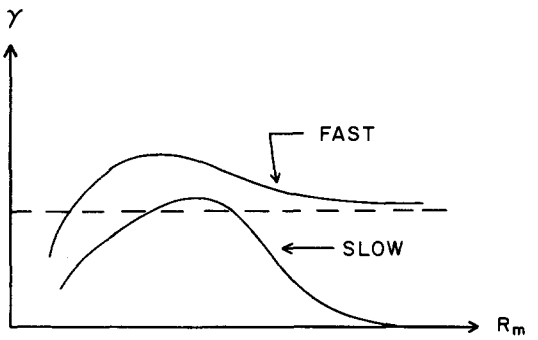

FIG. 1. A schematic illustrating the growth rate γ of fast and slow kinematic dynamos.

[a)] And Department of Electrical Engineering and Department of Physics.

 0031-9171/88/102992-20$01.90

tational approaches to the dynamo problem at large R_m (small η). (The work in Ref. 16 also addresses the dynamo problem using a map.)

In Sec. V we introduce a numerical method for studying the existence of fast dynamo action via the *zero resistivity* equation. The accuracy and limitations of the method are tested on the simple analytically tractable maps introduced in Sec. IV. Then the method is applied to a time-periodic flow, which we believe has features typical of those to be expected in practice. We find that here too the method is capable of yielding useful results.

To close this section we mention several issues not addressed in the formulation of the kinematic fast dynamo problem.

(i) The kinematic dynamo is a linear instability problem. If the magnetic field grows, the magnetic energy density will eventually become of the order of the kinetic energy density in the fluid flow. At this point the magnetic field will self-consistently react back through the Lorentz force to alter the flow velocity. The problem then becomes nonlinear, involving the full set of magnetohydrodynamic (MHD) equations. Thus, while a solution of the kinematic dynamo problem can reveal why magnetic fields are present, it cannot directly explain specific features observed in nonlinear states (e.g., the magnitude of the Earth's magnetic field, or properties, such as spatial scales of sunspots).

(ii) In order for magnetic fields to be generated by a kinematic dynamo, a small seed field must be present. One possibility for creating such a seed field is thermoelectric charges and currents driven by temperature gradients.[5]

(iii) Fast dynamos are argued to be important because $R_m = v_0 L_0 / \eta$ can be very large. In the calculation of these large R_m values the classical formula for the resistivity due to collisions is typically used. In plasmas with large currents and thermal and density gradients, however, kinetic instabilities (not described by the MHD equations) can occur. These instabilities can drive short wavelength modes, which generate a microturbulent state resulting in greatly enhanced resistivity.[17,18]

II. FAST DYNAMOS AND CHAOTIC FLOWS

We consider a fluid with velocity $\mathbf{v}$, current density $\mathbf{J}$, magnetic field $\mathbf{B}$, and electric field $\mathbf{E}$. Maxwell's equations (with displacement current neglected) together with Ohm's law, $\eta\mathbf{J} = \mathbf{E} + \mathbf{v}\times\mathbf{B}$ (where η is the resistivity), yield the following equation for the magnetic field:

$$\frac{\partial \mathbf{B}}{\partial t} - \nabla\times(\mathbf{v}\times\mathbf{B}) = \frac{1}{R_m}\nabla^2\mathbf{B},$$

where the spatial coordinates have been normalized to a characteristic length for variation of $\mathbf{v}$ (denoted L_0), $\mathbf{v}$ is normalized to its typical magnitude (denoted v_0), and the time t is normalized to L_0/v_0. For an incompressible flow ($\nabla\cdot\mathbf{v} = 0$), the above equation becomes

$$\frac{\partial \mathbf{B}}{\partial t} + \mathbf{v}\cdot\nabla\mathbf{B} = \mathbf{B}\cdot\nabla\mathbf{v} + \frac{1}{R_m}\nabla^2\mathbf{B}. \tag{1}$$

The basic kinematic dynamo problem is to solve this equation with a given velocity $\mathbf{v}(\mathbf{x},t)$. Generally, three classes of flows[11] have been considered: (1) steady time independent flows, $\mathbf{v} = \mathbf{v}(\mathbf{x})$; (2) time-periodic flows, $\mathbf{v}(\mathbf{x},t) = \mathbf{v}(\mathbf{x},t+T)$, where T is the time period; and (3) turbulent flows. Most of our specific considerations will be in the context of time-periodic flows, although we believe that some of our considerations (in particular, those in Sec. IV) also can be fruitfully applied to steady and turbulent flows. (The steady fast dynamo problem is particularly intriguing, since it is currently not definitely known whether one is possible for smooth flows.[8,9,12,14]) For the case of steady flow, we can take the field to be of the form $\mathbf{B} = \mathbf{b}(\mathbf{x})e^{st}$, $s = \gamma - i\omega_r$. For the case of a time-periodic dynamo flow, we can assume the Floquet form, $\mathbf{B} = \mathbf{b}(\mathbf{x},t)e^{st}$, with $\mathbf{b}(\mathbf{x},t) = \mathbf{b}(\mathbf{x},t+T)$. In either case, Eq. (1) yields an eigenvalue problem for the eigenvalues s and the eigenfunctions $\mathbf{b}$.

Formally taking the magnetic Reynolds number to infinity ($\eta = 0$) in Eq. (1) we have

$$\frac{\partial \mathbf{B}}{\partial t} + \mathbf{v}\cdot\nabla\mathbf{B} = \mathbf{B}\cdot\nabla\mathbf{v}. \tag{2}$$

This is a hyperbolic equation with characteristics that are the trajectories of fluid elements,

$$\frac{d\mathbf{x}(t)}{dt} = \mathbf{v}(\mathbf{x}(t),t). \tag{3}$$

It is instructive to consider a variation of $\mathbf{x}(t)$. That is, we consider two initial conditions, $\hat{\mathbf{x}}_0$ and $\hat{\mathbf{x}}_0 + \delta\mathbf{x}_0$, where the variation $\delta\mathbf{x}_0$ is an infinitesimal vector, and evolve these initial conditions under (3) to new positions $\hat{\mathbf{x}}(t)$ and $\hat{\mathbf{x}}(t) + \delta\mathbf{x}(t)$. The variation $\delta\mathbf{x}(t)$ satisfies the equation

$$\frac{d\delta\mathbf{x}}{dt} = \delta\mathbf{x}\cdot\nabla\mathbf{v}, \tag{4}$$

with $\mathbf{v} = \mathbf{v}(\hat{\mathbf{x}}(t),t)$. Comparing Eqs. (2) and (4), we see that $\mathbf{B}$ and $\delta\mathbf{x}$ satisfy the same equation. [This is a consequence of the frozen-in-field condition (e.g., Ref. 6).] Thus it has been suggested[8] that the exponential growth of $\mathbf{B}$ in a *fast* dynamo is connected with the exponential separation of nearby orbits of fluid elements. For an equation such as (3) and an initial condition $\hat{\mathbf{x}}_0$, the *Lyapunov exponent* is defined as

$$\lambda_L = \lim_{t\to\infty}(1/t)\ln[\,|\delta\mathbf{x}(t)|/|\delta\mathbf{x}_0|\,]. \tag{5}$$

Thus λ_L is the average exponential rate of separation of two nearby points. For a given $\hat{\mathbf{x}}_0$ this number is the same for almost any choice of the direction of $\delta\mathbf{x}_0$. (For special choices of the direction of $\delta\mathbf{x}_0$, other, smaller, values of λ_L result. Here we are only concerned with the largest λ_L.) Flows with $\lambda_L > 0$ for a nonzero volume set of $\hat{\mathbf{x}}_0$ are said to be chaotic. Thus chaotic flows are good candidates for fast dynamos. In addition to the Lyapunov number, another quantitative characterization of a flow is the *topological entropy*, which, for our purposes, we define

$$\lambda_T = \max_{l_0}\lim_{t\to\infty}(1/t)\ln[\,\|l(t)\|/\|l_0\|\,], \tag{6}$$

where l_0 denotes a finite length curve, $l(t)$ is the image of this curve under the flow (i.e., the curve that results by following the trajectory of each fluid element on l_0 from time zero to time t), and $\|l_0\|$ and $\|l(t)\|$ are the lengths of these curves. Thus λ_T is the maximum exponential rate of increase of the

length of a curve. In general, the inequality

$$\lambda_T \geqslant \lambda_L$$

holds. As we shall discuss further, λ_T can exceed λ_L if there is nonuniformity in the rate of stretching.

In Eq. (6) we have taken the topological entropy to be the maximum exponential rate of growth of a line segment. Actually, for a three-dimensional flow the conventional definition of λ_T yields[19] the larger of the maximum rate of exponential growth of a line or of an area. Roughly speaking, if the flow is stretching in only one direction then Eq. (6) coincides with the conventional topological entropy, while if it is stretching in two directions then area growth gives the conventional topological entropy. For a two-dimensional area preserving map or a *steady* incompressible flow, areas do not expand faster than lines and Eq. (6) coincides with the conventional topological entropy. For time-periodic flows or three-dimensional volume preserving maps, it is possible that areas can expand faster than lines, and then our definition, Eq. (6), would not coincide with the conventional topological entropy. Nevertheless, in the remainder of this paper we will take the term topological entropy to mean the rate of exponentiation of a line, i.e., Eq. (6).

III. RELEVANCE OF THE ZERO RESISTIVITY EQUATION

We now wish to discuss the sense in which the solution of Eq. (2) [which is the $\eta = 0$ version of Eq. (1)] is relevant to the solution of Eq. (1) with a small but nonzero η. To begin we assume that a fast dynamo exists and estimate the smallest scale ξ generated by Eq. (1) with finite resistivity. We have the following orderings: $\nabla \mathbf{B}/\mathbf{B} \sim \xi^{-1}$ and $\nabla^2 \mathbf{B}/\mathbf{B} \sim \xi^{-2}$; due to the normalizations, $\nabla \mathbf{v} \sim 1$; since in the zero resistivity limit, $d\mathbf{B}/dt \equiv \partial \mathbf{B}/\partial t + \mathbf{v}\cdot\nabla\mathbf{B}$ balances $\mathbf{B}\cdot\nabla\mathbf{v}$ [Eq. (2)], we have $B^{-1} d\mathbf{B}/dt \sim 1$. Thus the resistive term sets the scale at[10]

$$\xi \sim R_m^{-1/2}.$$

The action of the resistance is to smooth (i.e., diffuse) magnetic flux over the scale ξ during a growth time [which is $O(1)$ for a fast dynamo]. However, on length scales long compared to ξ the spatially averaged flux is little changed by the diffusion during a growth time. (Note that this diffusion implies magnetic reconnection when oppositely directed fields occur within a distance of the order of ξ of each other.) Hence if we look at a surface S and calculate the flux through it,

$$\Phi_S = \int_S \mathbf{B}\cdot d\mathbf{A},$$

then we expect Φ_S for the exponentiating field to be independent of R_m as long as the dimensions of S are large compared to ξ. Thus consider the rate of growth of flux through S calculated from Eq. (1) with magnetic Reynolds number R_m,

$$\tilde{\Gamma}_S(R_m) = \lim_{t\to\infty} \sup (1/t) \ln |\Phi_S(t)/\Phi_S(0)|, \tag{7}$$

and the corresponding quantity calculated using the *perfectly conducting* equation (2). We denote the latter quantity Γ_S. We expect $\tilde{\Gamma}_S(R_m)$ to be the instability growth rate for the fastest growing mode at R_m for typical choices of S and $\mathbf{B}_0(\mathbf{x})$, where $\mathbf{B}_0(\mathbf{x})$ is the initial seed magnetic field which we assume to be a smooth function of $\mathbf{x}$. Since we have argued that, for any given surface S, the flux Φ_S is independent of R_m for large enough R_m (i.e., small enough ξ), we conjecture that

$$\lim_{R_m\to\infty} \tilde{\Gamma}_S(R_m) = \Gamma_S \tag{8}$$

(assuming the limit exists as in Fig. 1). In particular, Eq. (8) claims that the high magnetic Reynolds number instability growth rate can be calculated by using the perfect conductivity equation (2) to obtain Γ_S. Furthermore, there is, or is not, a fast magnetic dynamo for a given flow, $\mathbf{v}(\mathbf{x},t)$, according to whether Γ_S is positive or not. In the remainder of this paper we deal with the zero resistivity dynamo equation (2).

Before proceeding, however, we offer some comments on the above discussion.

(i) A flow may have several disjoint ergodic chaotic components, each with a different λ_L. In such a case, it seems reasonable that an eigenfunction of (1) would typically be confined to one such component in the limit $R_m \to \infty$.

(ii) It is necessary to use lim sup rather than simply lim in Eq. (7) to accommodate the possibility of a real frequency for the fastest growing mode.

(iii) An alternative formulation of Eq. (8) is that the $t\to\infty$ and the $R_m \to \infty$ limits of the flux exponentiation rate are interchangeable:

$$\lim_{R_m\to\infty} \limsup_{t\to\infty} [(1/t)\ln|\Phi_S(t)/\Phi_S(0)|]$$

$$= \limsup_{t\to\infty} \lim_{R_m\to\infty} [(1/t)\ln|\Phi_S(t)/\Phi_S(0)|].$$

(iv) One does not need to speak of magnetic fields to define Γ_S: we can take the flux to be that of $\delta\mathbf{x}$ instead of $\mathbf{B}$, $\Phi_S = \int_S \delta\mathbf{x}\cdot d\mathbf{A}$, and Γ_S is unchanged. Thus, like the Lyapunov exponent and the topological entropy, Γ_S is purely a dynamical property of the flow $\mathbf{v}(\mathbf{x},t)$. Although λ_L and λ_T are basic quantities in the ergodic theory of dynamical systems, Γ_S seems not yet to have appeared in this context.

(v) Let ω be the fluid vorticity, $\omega = \nabla\times\mathbf{v}$. Then, the evolution of ω in an ordinary uniform density incompressible fluid (without magnetic fields) is given by

$$\frac{\partial\omega}{\partial t} + \mathbf{v}\cdot\nabla\omega = \omega\cdot\nabla\mathbf{v} + \frac{1}{R}\nabla^2\omega,$$

where R is the Reynolds number, $R = L_0 v_0/\mu$, and μ is the viscosity. This equation is formally the same as Eq. (1). The difference is, of course, that for the kinematic dynamo problem we can take $\mathbf{v}$ to be specified; here ω equals $\nabla\times\mathbf{v}$ and produces an inherently nonlinear equation. Nevertheless, there are similarities in the results for the two problems, and these may be caused by the identical forms of the equations. Specifically, in fully developed fluid turbulence there is a cascade to smaller scale eddies, which occupy a smaller and smaller fraction of the space (intermittency) eventually (it is thought) concentrating on a fractal set as $R\to\infty$ (cf. Refs. 20–23). Our baker's maps in Sec. IV may thus have some relevance to the fluid turbulence problem.

(vi) Although it is conjectured that chaos is necessary

for a fast dynamo of a spatially smooth flow,[14] the presence of chaos does not guarantee dynamo action. In particular, consider the special case of a time-periodic, two-dimensional, incompressible velocity,

$$\mathbf{v} = \nabla\phi \times \mathbf{z}_0, \quad \mathbf{x} = (x,y), \quad \phi(x,y,t) = \phi(x,y,t+T).$$

Then $d\mathbf{x}/dt = \mathbf{v}$ yields a map, $\mathbf{x}[(n+1)T] \equiv \mathbf{x}_{n+1} = \mathbf{F}(\mathbf{x}_n)$. Choosing for the streamfunction

$$\phi(x,y,t) = \phi_1(x)\sum_m \delta(t - mT - \epsilon) + \phi_2(y)\sum_m \delta(t - mT - 2\epsilon),$$

where ϵ is a small positive quantity, we have the map $x_{n+1} = x_n + \phi_2'(y_n)$, $y_{n+1} = y_n - \phi_1'(x_{n+1})$, where the prime denotes differentiation. For $\phi_1' = -x$, $\phi_2' = K \sin y$, this is the well-known standard map extensively used as a model for Hamiltonian chaos. However, even though the flow may be chaotic, no dynamo is possible in two dimensions (this is related to "Cowling's theorem," e.g., Ref. 6). One can also obtain an analogous result for *steady* space periodic flows with $\nabla v_z = 0$:

$$\mathbf{v} = \nabla\phi \times \mathbf{z}_0 + v_0\mathbf{z}_0,$$

where $\phi(x,y,z) = \phi(x,y,z+L)$. These flows also cannot be dynamos (cf. Appendix A) but can be chaotic (e.g.,

$$\phi = v_0\sum_m [\phi_1(x)\delta(z - mL - \epsilon) + \phi_2(y)\delta(z - mL - 2\epsilon)]$$

yields the same two-dimensional map as previously for the transverse position (x_n, y_n) at z locations $z_n = nL = nv_0T$). For a further discussion of this latter case see Appendix A. Also, Ref. 16 demonstrates antidynamo behavior (i.e., $\Gamma_s < 0$) in the three-dimensional chaotic flows.

(vii) For flows that are not incompressible, the continuity equation [$\partial\rho/\partial t + \nabla\cdot(\rho\mathbf{v}) = 0$, where ρ is the mass density] yields in place of Eq. (1),

$$\frac{\partial}{\partial t}\frac{\mathbf{B}}{\rho} + \mathbf{v}\cdot\nabla\left(\frac{\mathbf{B}}{\rho}\right) = \frac{\mathbf{B}}{\rho}\cdot\nabla\mathbf{v} + \frac{1}{\rho R_m}\nabla^2\mathbf{B}.$$

Thus the zero resistivity equation is the same for incompressible flows and for compressible flows (with the replacement $\mathbf{B} \to \mathbf{B}/\rho$). Furthermore, for large R_m the length scale of $\mathbf{B}$, $\xi \sim R_m^{-1/2}$, is much less than that of ρ. (We assume that the density is self-consistently evolved by the fluid equations and therefore has length scales unrelated to R_m.) Hence for large R_m, $\rho^{-1}\nabla^2\mathbf{B} \cong \nabla^2(\mathbf{B}/\rho)$, and the compressible problem is the same as the incompressible problem. This is significant because some flows thought to lead to dynamo action are compressible (for example, Rayleigh–Bénard convection cells in the sun).

(viii) Support for our conjecture, Eq. (8), comes from the stretch–twist–fold examples that we treat in Sec. IV. In particular, if we regard the stretch–twist–fold operation to be done impulsively at times $t = nT$ ($n = 0,1,2,...$, and we take $T \sim 1$ in our normalized units), then finite resistivity has no effect during the impulse. Between impulses we have $\partial\mathbf{B}/\partial t = R_m^{-1}\nabla^2\mathbf{B}$ (i.e., the field evolves purely diffusively), and the field will be smoothed over the scale $\xi \sim R_m^{-1/2}$. Thus, between the impulses, Φ_S will be little changed by flux diffusion if the dimensions of S are much greater than ξ. Furthermore, for these examples, when the impulse is next applied, the smoothing has little effect: The total flux through the torus in the examples is doubled *independently* of the distribution of flux within the torus.

(ix) Since the normalized equation without resistivity, Eq. (2), has no dimensionless parameters, the growth rate of the magnetic flux in normalized time is of order unity. That is, in the dimensional units, the growth rate is of the order of v_0/L_0, the ratio of the typical velocity to the typical length scale of the flow. For example, if the flow arises from Rayleigh–Bénard convection (i.e., the flow induced by the heating of a fluid layer from below in the presence of gravity), one would estimate the fast dynamo growth rate to be of the order of the turnover time of the resulting convective rolls.

IV. MODELS

The linear stability problem posed by the kinematic dynamo problem [Eq. (1)], requires the specification of the velocity field $\mathbf{v}(\mathbf{x},t)$ (which constitutes the zeroth-order state about which the linearization is performed). Ideally, one might desire to utilize a specific fluid flow arising from realistic flows in specific situations (for example, the Rayleigh–Bénard thermal convection cells in the sun's convection zone). In practice, this would be extremely difficult. Our approach in this section will be less ambitious and is similar to that followed by others. Specifically, we shall specify *model* flows that allow the possibility of analysis. The idea is that the results so obtained will have general features to be expected in fast kinematic dynamos that arise from more realistic flows and that we can relate these features to features of the flow. In particular, we will topologically specify certain flows (called stretch–twist–fold dynamos[5]), which are chaotic in the sense discussed in Sec. II. We subsequently argue that certain properties of these analyzable models are to be expected, in general, when one encounters realistic flows that are chaotic. Evidence in support of this statement is provided by the numerical computations of Sec. V C.

A. The stretch–twist–fold process and baker's maps

The paradigmatic model fast dynamo[5] is illustrated in Fig. 2. At $t = 0$ there is a toroidal flux tube with a circulating flux Φ_0 [Fig. 2(a)]. The tube is then uniformly stretched to twice its original length [Fig. 2(b)]. Since the fluid is incompressible, the tube cross-sectional area is now half of what it was in Fig. 2(a). Since the magnetic field is frozen-in, the circulating flux in the stretched tube is still Φ_0. The tube is then twisted into a figure eight [Fig. 2(c)], and folded back into the original volume occupied by the tube in Fig. 2(a) [Fig. 2(d)]. The total circulating flux is $2\Phi_0$. Repeating this sequentially, the circulating flux doubles each time producing a flux growth rate $\Gamma = (\ln 2)/T$, where T is the period of the cycle. [The repeated application of the process in Fig. 2 can be regarded as specifying a periodic velocity field $\mathbf{v}(\mathbf{x},t) = \mathbf{v}(\mathbf{x},t+T)$.]

Now say we follow the process in Fig. 2, but do the stretching in a nonuniform way. Figure 3 illustrates an example of what we mean by this. We start as before, Fig. 3(a),

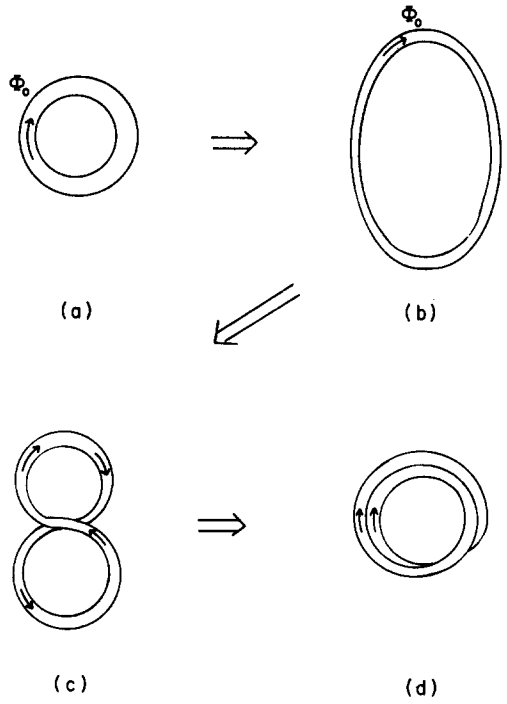

FIG. 2. The stretch–twist–fold fast dynamo.

but now divide the tube into two unequal pieces, one taking up a fraction $\alpha < \frac{1}{2}$ of the circumference, the other a fraction β, with $\alpha + \beta = 1$. We then stretch the lower piece by a factor $1/\alpha$ and the upper piece by $1/\beta$. The lower and upper pieces each now have the length of the original circumference. Because of incompressibility, their cross-sectional areas are now, respectively, α and β times their original areas [Fig. 3(b)]. Twisting and folding, as before, we again double the flux but in a nonuniform way. That is, if we now look at a cross section of the loop after the fold [Fig. 3(c)], it will consist of a small area αA and a larger area βA [where A is the original cross section in Figs. 2(a) and 3(a)]. Each of these two component areas has the same flux through it (namely, Φ_0), and the field is higher in the α area than in the β area. Again the total flux is doubled and it continues to be doubled on each repeated subsequent application of the operations in Fig. 3. Thus the flux growth rate is again $(\ln 2)/T$.

What happens to the distribution of magnetic flux in a cross section if the process in Fig. 3 is repeated many times? To understand this (cf. Sec. IV B) we abstract the process slightly by considering the two-dimensional map in Fig. 4. Here we consider a perfectly conducting square sheet and imagine that there is a uniform upward directed magnetic field in the sheet. [The y direction in Fig. 4(a) is analogous to the toroidal direction in Fig. 3(a).] We now give the square an incompressible deformation: we horizontally compress the lower part of the square ($0 < y < \alpha$) by a factor α and vertically stretch it by $1/\alpha$; thus the area is conserved (incompressible). Simultaneously we horizontally compress the upper part of the square ($\alpha < y < 1$) by β and vertically stretch it by $1/\beta$ where $\beta = 1 - \alpha$. This is illustrated in Fig. 4(b). We then separate the two parts and cut the magnetic field lines between them [Fig. 4(c)]. The two pieces are then reassembled into the original square [Fig. 4(d)]. The operation of cutting the field lines is nonphysical, but is introduced to simulate the three-dimensional stretch–twist–fold operation. It is this cutting of field lines that allows the modeling of an inherently three-dimensional process by a two-dimensional map. [Indeed according to comment (vi) at the end of Sec. III, physical dynamos are impossible in two dimensions.] Since the field is frozen-in, the flux through a horizontal line ($y = \text{const}$) across the α strip and the flux through a horizontal line across the β strip are each the same as the flux through a horizontal line ($y = \text{const}$) across the entire square in Fig. 4(a). Thus the flux across the whole square in Fig. 4(d) is double that in Fig. 4(a), as is the case for the nonuniform stretch–twist–fold operation of Fig. 3. Also the ratio of the area that contains high field to the area of low field is α/β for Fig. 4. Likewise, for Fig. 3 the ratio of the volume containing high field to that containing low field is also α/β.

Analytically we can express the map in Fig. 4 as

$$x_{n+1} = \begin{cases} \alpha x_n, & \text{if } y_n < \alpha, \\ \beta x_n + \alpha, & \text{if } y_n > \alpha; \end{cases} \tag{9a}$$

$$y_{n+1} = \begin{cases} y_n/\alpha, & \text{if } y_n < \alpha, \\ (y_n - \alpha)/\beta, & \text{if } y_n > \alpha. \end{cases} \tag{9b}$$

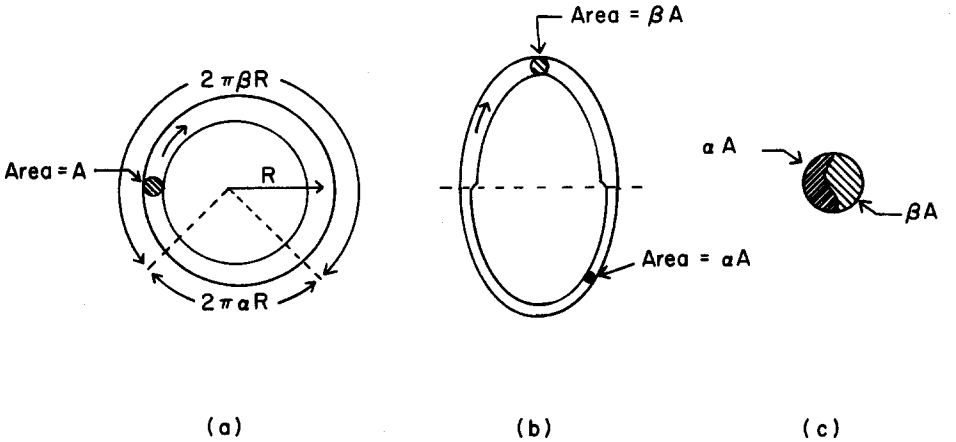

FIG. 3. Nonuniform stretch–twist–fold. In (b) the lengths above and below the dashed line are both the original length, $2\pi R$. Part (c) shows the cross section after the fold operation; the flux in the αA and βA areas is the same, and thus the field strength in the smaller αA area is larger.

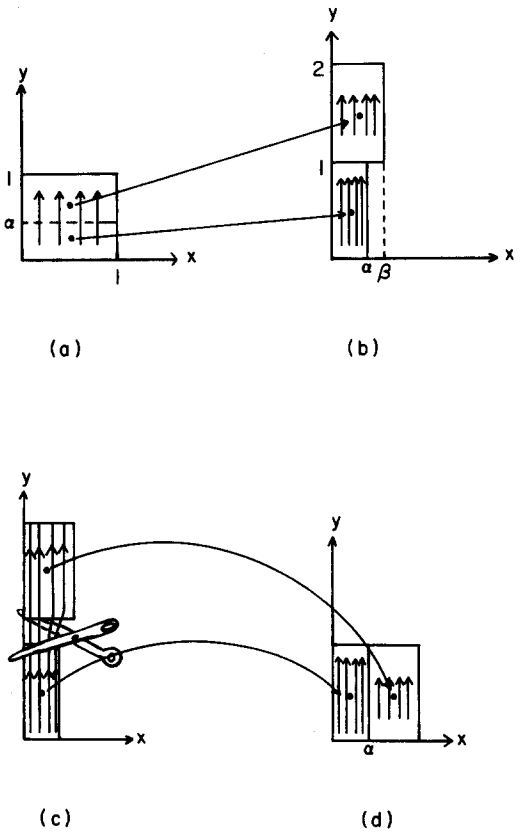

FIG. 4. Two-dimensional baker's map of Eq. (9) corresponding to the stretch–twist–fold of Fig. 3. The operation of cutting the field lines in (c) allows the three-dimensional property of flux alignment (Fig. 3) in a two-dimensional map.

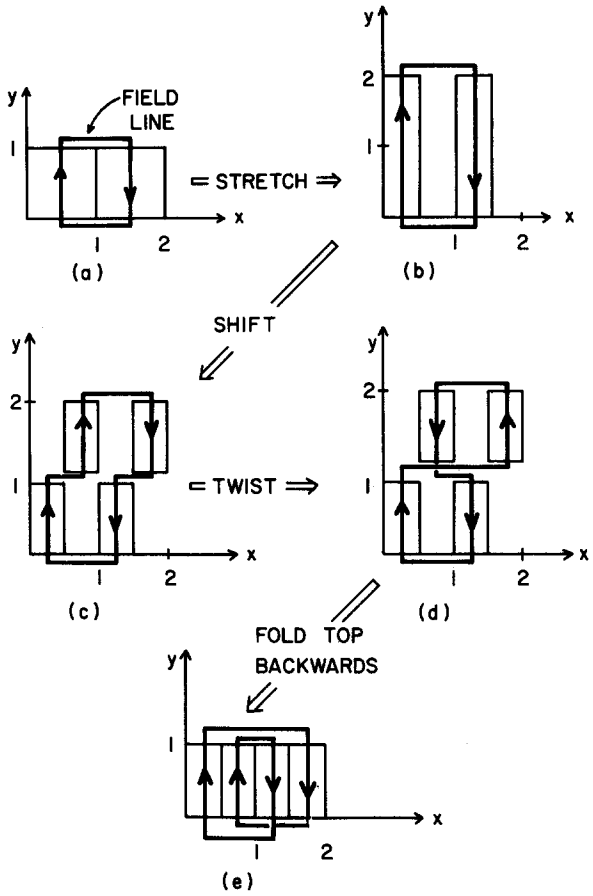

FIG. 5. This figure is essentially the same as the stretch–twist–fold illustrated in Fig. 3, except that we imagine the torus of Fig. 3(a) to be beaten into a thin sheet. The hole in the center of the torus is now the slit from (1,0) to (1,1) [Fig. 5(a)]. The net result at the end of the cycle (a)–(e) is that the state of the square $1\geqslant(x,y)\geqslant 0$ in (a) is related to that in (e) by the map in Fig. 4 and Eq. (9).

For another justification of Eq. (9) as a model of the process in Fig. 3, see Fig. 5 and its caption. [The map, Eq. (9), is a special case of a class of maps called generalized baker's maps, which were introduced in Ref. 24 for the study of strange attractors.]

In the processes illustrated in Figs. 2–4 the magnetic fluxes in the two components add when the process is completed [e.g., the **B** in the α strip and the **B** in the β strip are both upward in Fig. 4(d)]. In Fig. 6 we illustrate an operation on a flux loop wherein some cancellation of flux is produced after the completion of the process. The loop is stretched, perhaps nonuniformly, to four times its original circumference [Fig. 6(b)]. The lower quarter is given a twist [Fig. 6(c)], and then the result is folded back into its original volume. The first part of the folding operation is illustrated by the double arrows in Fig. 6(c) and its result appears in Fig. 6(d). The final folding is indicated by the double arrow in Fig. 6(d). Figure 7 shows a baker's map corresponding to Fig. 6. Figure 7(a) shows an initially uniform upward directed magnetic field in the unit square. The square is composed of four horizontal strips of varying heights $(\alpha,\beta,\gamma,\delta)$ with $\alpha+\beta+\gamma+\delta=1$. Each strip is given an incompressible vertical stretching, so that each is now one unit long [Fig. 7(b)]. We then imagine the flux lines to be cut [as in Fig. 4(c)] at $y=1$, $y=2$, and $y=3$. Then the strip between $y=2$ and $y=3$ is rotated 180°, so that its magnetic field is pointed downward, and the four strips are then put back in the unit square [Fig. 7(c)]. Analytically, Fig. 7 is the map,

$$x_{n+1}=\begin{cases}\alpha x_n, & \text{if } 0<y_n<\alpha,\\ \beta x_n+\alpha, & \text{if } \alpha<y_n<(\alpha+\beta),\\ \gamma(1-x_n)+\alpha+\beta, & \text{if } (\alpha+\beta)<y_n<(\alpha+\beta+\gamma),\\ \delta x_n+\alpha+\beta+\gamma, & \text{if } (\alpha+\beta+\gamma)<y_n<1;\end{cases} \tag{10a}$$

$$y_{n+1}=\begin{cases}y_n/\alpha, & \text{if } 0<y_n<\alpha,\\ (y_n-\alpha)/\beta, & \text{if } \alpha<y_n<(\alpha+\beta),\\ [(\alpha+\beta+\gamma)-y_n]/\gamma, & \text{if } (\alpha+\beta)<y_n<(\alpha+\beta+\gamma),\\ [y_n-(\alpha+\beta+\gamma)]/\delta, & \text{if } (\alpha+\beta+\gamma)<y_n<1.\end{cases} \tag{10b}$$

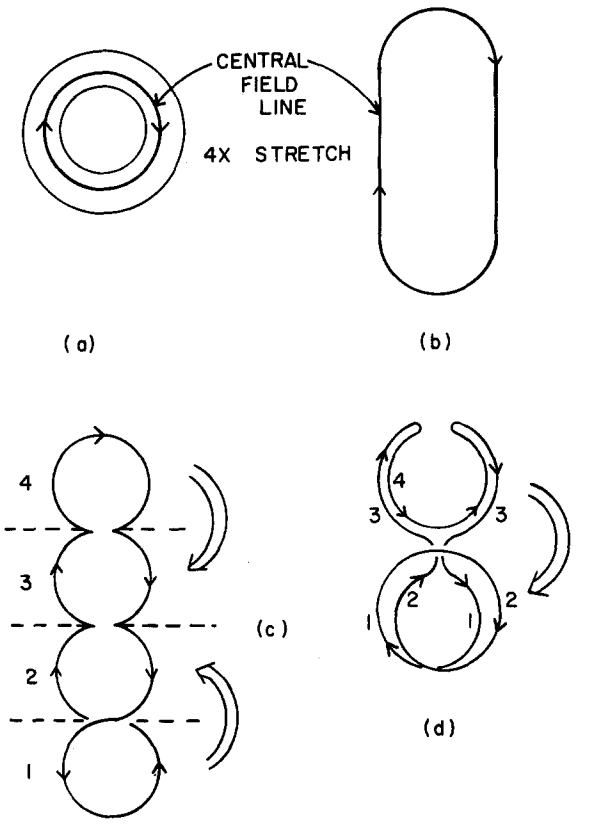

FIG. 6. Deformation of a flux loop into itself with flux amplification and partial cancellation. For clarity only the central flux line is shown in (b)–(d). The final fold indicated by the double arrow in (d) restores the flux to the volume occupied by the original loop.

Each strip in Fig. 7(c) has the original amount of flux in it, but the direction has been reversed in the third strip. Hence the total upward flux across the square in Fig. 7(c) is twice the original flux, and repeated applications of the process double the flux on each cycle. Thus the exponential flux growth rate is again $\Gamma = (\ln 2)/T$.

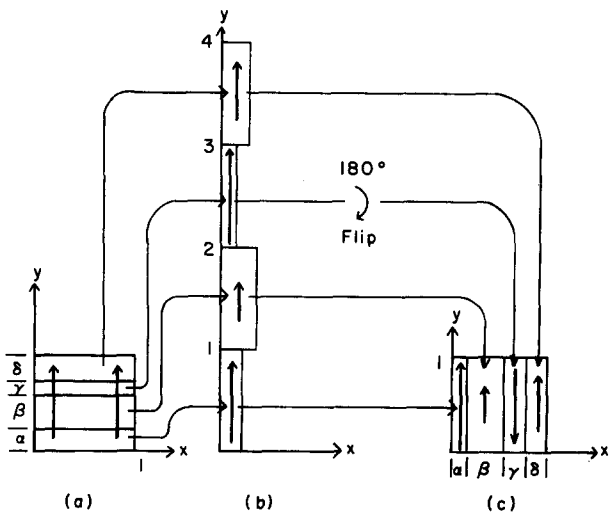

FIG. 7. Baker's map corresponding to Fig. 6. The four strips in (b) correspond to loops 1–4 in Fig. 6(c).

If the third strip had not been flipped, the total upward flux in Fig. 7(c) would be four times the original flux, and the exponential flux growth rate would have been $\Gamma = (\ln 4)/T$.

Cancellation can be included in two-strip baker maps like that of Fig. 4 by flipping the β strip, or in stretch–twist–fold cycles like that of Fig. 3 by omitting the twisting process. For these two-strip maps, the total flux exactly cancels in one iteration.

In the following subsections, we analyze the baker's maps (9) and (10) and on this basis we draw some general conclusions concerning fast dynamos.

B. Lyapunov exponents and topological entropy

The Lyapunov exponent of the map Eq. (9) (Fig. 4) is[24]

$$\lambda_L = \frac{\alpha \ln(1/\alpha) + \beta \ln(1/\beta)}{T}. \tag{11}$$

From Eq. (5) we see that λ_L is $1/T$ times the average of the logarithm of the stretch per iterate. Thus Eq. (11) can be obtained if we view orbit points to be random and uniformly distributed in y. Then the probability of an orbit point being in $0<y<\alpha$ is α, and the probability of it being in $\alpha<y<\alpha+\beta=1$ is β. Thus Eq. (11) shows that the average logarithm of the stretch per cycle is the probability of a stretch α^{-1} multiplied by $\ln \alpha^{-1}$ plus the probability of a stretch β^{-1} multiplied by $\ln \beta^{-1}$. Similarly, for the map Eq. (10) (Fig. 7),

$$\lambda_L = \frac{\alpha \ln(1/\alpha) + \beta \ln(1/\beta) + \gamma \ln(1/\gamma) + \delta \ln(1/\delta)}{T}. \tag{12}$$

Maximizing Eq. (11) subject to $\alpha+\beta=1$, we find the maximum λ_L is $\ln(2)/T$, which occurs at $\alpha=\beta=\frac{1}{2}$; similarly maximizing Eq. (12) subject to $\alpha+\beta+\gamma+\delta=1$, the maximum λ_L is $\ln(4)/T$ occurring at $\alpha=\beta=\gamma=\delta=\frac{1}{4}$. In both cases λ_L is largest, and equal to λ_T, when the stretching is uniform (i.e., the same in each strip).

To obtain the topological entropy for the maps (9) and (10) it suffices to consider an initially vertical line running from $y=0$ to $y=1$. Equation (6) then yields

$$\lambda_T = (\ln 2)/T \tag{13}$$

for the map of Eq. (9), and

$$\lambda_T = (\ln 4)/T \tag{14}$$

for the map of Eq. (10). Comparing Eqs. (11)–(14) with the exponential flux growth rates Γ, we have the following: (i) $\lambda_T = \Gamma$ for Eq. (9); (ii) $\lambda_T > \Gamma$ for Eq. (10); (iii) λ_T would be the same as Γ if the flip had not been introduced in Eq. (10); (iv) $\lambda_L \leqslant \lambda_T$ for both Eqs. (9) and (10) with the equality holding only when the stretching is uniform; and (v) λ_L can exceed Γ for the map of Eq. (10) [depending on $(\alpha,\beta,\gamma,\delta)$].

Thus λ_L can be either larger or smaller than the maximum flux growth rate Γ. In contrast, however, the topological entropy seems to be more closely connected to Γ. We conjecture that, in general,

$$\lambda_T \geqslant \Gamma, \tag{15}$$

with the equality applying when cancellations are absent

(we expect the absence of cancellations to be an exceptional case for typical flows encountered in practice). This conjecture is based upon the idea that the dynamo growth rate, as computed by Eq. (8), is less than or equal to the growth rate of the "flux without cancellation,"

$$\tilde{\Phi}_S = \int_S |B_n| dA,$$

where B_n is the component of $\mathbf{B}$ normal to S. The topological entropy, as defined in Eq. (6), is the exponential rate of increase of a sum $\Sigma|\delta\mathbf{x}_i(t)|$, where the vectors $\delta\mathbf{x}_i$ are lined up, head to tail, to form the curve[25] $l(t)$. On the other hand, $\tilde{\Phi}_S$ is, by the equivalence of Eqs. (2) and (4), proportional to a similar sum, but where the tails of the vectors $\delta\mathbf{x}_i$ are distributed over the surface S. If all the points $\mathbf{x}_i$ are located in the same ergodic component, it seems reasonable that there should be no distinction, as $t\to\infty$, between points distributed along a curve or on a surface.

The Lyapunov exponent λ_L and the topological entropy λ_T satisfy $\lambda_L \leqslant \lambda_T$ with equality only for uniform stretching because λ_L is the average of the exponential rate of stretching of $\delta\mathbf{x}$ and λ_T is the exponential rate of stretching of the average of $\delta\mathbf{x}$ (the log of the average of a quantity is greater than or equal to the average of the log of the quantity).

C. Generation of small scales

In this subsection we consider the map Eq. (9) (Fig. 4) as an example illustrating the generation of small scales in chaotic fast dynamos. On one application of the map we generate two strips [Fig. 4(d)], one of width α and one of width β. Now apply the map again. Each of the two strips is stretched and compressed resulting in four strips, one of width α^2, one of width β^2, and two of width $\alpha\beta$. For n applications of the map, we produce 2^n strips of varying widths, $\alpha^{n-m}\beta^m$ $(m = 0,1,2,...,n)$. The number of strips at time nT having width $\alpha^{n-m}\beta^m$ is given by the binomial coefficient,[24]

$$Z(n,m) = n!/m!(n-m)!.$$

For large n, $Z(n,m)$ is approximately Gaussian in m (this follows from Stirling's approximation),

$$Z(n,m) \cong \frac{2^n}{\sqrt{2\pi}} \frac{1}{\sqrt{n/4}} \exp\left[-\frac{1}{2}\left(\frac{m-(n/2)}{\sqrt{n/4}}\right)^2 \right]$$

for $|(m/n) - \frac{1}{2}| \ll 1$. Thus, for large n, the quantity Z as a function of m is strongly peaked around $m = n/2$ with a width $\sim\sqrt{n}$. In particular, if we pick some fraction θ, then for large n we can say that a fraction $\theta < 1$ of the 2^n strips have m values that lie within the relatively narrow range $\frac{1}{2} + r/\sqrt{n} > (m/n) > \frac{1}{2} - r/\sqrt{n}$ (where r depends only on θ). These strips all have roughly the same width, $W_n \equiv \alpha^{n/2}\beta^{n/2}$. Furthermore, since each of the 2^n strips contains the same flux (whatever its width), these strips contain θ of the total flux. Thus the strips containing a fraction θ of the flux occupy a total length in x of the order of

$$2^n\theta(\alpha\beta)^{n/2} = [2\sqrt{\alpha(1-\alpha)}\,]^n\theta.$$

If the stretching is nonuniform $(\alpha \neq \frac{1}{2})$, then the quantity $2[\alpha(1-\alpha)]^{1/2}$ is less than unity. Thus the flux is concentrated on a set whose total length in x tends exponentially to zero with time (i.e., increasing n).

In fact this $n\to\infty$ limit set is a fractal whose dimension we can calculate. One definition of the dimension[24] of a set is the capacity (or box-counting) dimension, which we denote D_c. If the set lies in an M-dimensional Euclidean space, D_c is defined as

$$D_c = \lim_{\epsilon\to 0}[\ln N(\epsilon)/\ln(1/\epsilon)], \tag{16}$$

where $N(\epsilon)$ is the minimum number of M-dimensional cubes of edge length ϵ needed to cover the set. (In one dimension, $M = 1$, the "cube" is an interval of length ϵ.) To calculate the capacity dimension of the smallest set (along the x axis), which in the limit as $n\to\infty$ contains a fraction θ of the flux, we set $\epsilon = W_n = (\sqrt{\alpha\beta}\,)^n$. Then from the previous discussion, $N(\epsilon) \sim 2^n\theta$, and we obtain a fractal dimension,

$$D_c(\theta) = (\ln 2)/\ln(1/\sqrt{\alpha\beta}\,), \tag{17}$$

which is, in general (i.e., for $\alpha \neq \frac{1}{2}$), less than unity. Note that Eq. (17) is independent of θ for $0 < \theta < 1$. For further discussion and other concepts of fractal dimension[24,26] see Appendix B.

For general chaotic flows, nonuniform stretching is generic. Thus we expect that flux concentration on a fractal is typical for fast dynamos in the $R_m \to \infty$ limit.

If at $n = 0$ we start off with a uniform upward directed magnetic field B_0, then at iterate n of the map Eq. (9) there are 2^n strips in each of which the magnetic field takes on one of the values $B(n,m) = B_0/(\alpha^{n-m}\beta^m)$, for $m = 0,1,2,...,n$. Assume we choose a point at random in the interval $0 \leqslant x \leqslant 1$. What is the probability that the magnetic field at this point is $B(n,m)$? Since strips with this magnetic field have width $\alpha^{n-m}\beta^m$ and number $Z(n,m)$, this probability is $P(n,m) = \alpha^{n-m}\beta^m Z(n,m)$. Again, using Stirling's approximation we obtain for large n

$$P(n,m) \cong (1/\sqrt{2\pi n\alpha\beta}\,)\exp[-(m-n\beta)^2/2n\alpha\beta]$$

for $|m/n - \beta| \ll 1$. Expressing m in terms of $B(n,m)$, we see that m is linearly related to the logarithm of $B(n,m)$,

$$m = n\frac{\ln\alpha}{\ln(\alpha/\beta)} + \frac{\ln[B(n,m)/B_0]}{\ln(\alpha/\beta)}.$$

Thus, since $P(n,m)$ is approximately Gaussian, the probability distribution of the magnetic field at randomly chosen points will be approximately lognormal in the long time limit. [Note, however, that the far tails of the lognormal will not yield accurate results, since our Gaussian approximation to $P(n,m)$ is only good for $|m/n - \beta| \ll 1$.] This approximate lognormal property, although obtained above for a specific model [Eq. (9)], can be plausibly argued to be a general property of chaotic fast dynamos. The argument is as follows. Lognormal distributions result from the multiplication of many random numbers, a simple consequence of the central limit theorem. As we integrate the chaotic trajectory, the net stretchings of $\delta\mathbf{x}$ experienced within blocks of time larger than a correlation time are essentially independent and random. Thus, since the stretching process is essentially multiplicative, we may expect that the long time field distribution is lognormal. (For related discussions of lognormality within the context of fluid turbulence and strange attractors, see Refs. 20 and 24.)

We now comment on the time evolution of the magnetic energy for this model and the effect of finite R_m. As argued in Sec. III, the diffusive nature of Eq. (1) implies that the growth of flux through a surface is insensitive to R_m as long as R_m is large enough. This is not so for the magnetic energy. For Eq. (9) the magnetic energy $U=\int_0^1\int_0^1(\mathbf{B}^2/2)dx\,dy$ at time nT is related to that at time $(n+1)T$ by

$$U_{n+1}=(\alpha^{-1}+\beta^{-1})U_n=(\alpha\beta)^{-1}U_n,$$

or $U_n=U_0\exp(2\gamma_E nT)$, where

$$\gamma_E=T^{-1}\ln(1/\sqrt{\alpha\beta})\geqslant T^{-1}\ln 2$$

with the equality applying only for $\alpha=\beta$. Thus we expect, in general, $\gamma_E\geqslant\lambda_T\geqslant\Gamma$, with equality only for uniform stretching. For finite resistivity, the magnetic energy initially grows according to $\exp(2\gamma_E nT)$ until the scale length approaches $\xi\sim R_m^{-1/2}$ (see Sec. III). After a transition period, the energy should then grow as $\exp(2\Gamma nT)$, $\Gamma=(\ln 2)/T$. Essentially what happens is that, during the initial phase, the scale for variation of **B** decreases exponentially. These rapid variations of **B** imply large currents, that, through resistivity, lead to enhanced dissipation which eventually slows the growth of U to $\exp(2\Gamma nT)$. Thus when looking at the zero resistivity *limit* of the growth rate via the equation for **B** with zero resistivity (2), it is important to examine the time evolution of flux through a surface rather than the time evolution of the magnetic energy. This is because the former is insensitive to R_m for large R_m, while the latter is not. [Another indication of why energy should not be considered is that the fractal measure giving the magnetic flux eigenfunction (Appendix B) has infinite magnetic energy.]

D. Tendency for cancellation

We consider the map (10) (Fig. 7). After n iterates of the map, we will have 4^n vertical strips. The *magnitude* of the flux in each strip will be the original upward flux Φ_0. Let N_+ be the number of strips at time nT with upward flux, and N_- the number with downward flux. The total flux doubles on each iterate. After n iterates we have

$$2^n\Phi_0=(N_+-N_-)\Phi_0,$$

$$N_++N_-=4^n.$$

Thus

$$\frac{N_+}{N_++N_-}=\frac{1}{2}+\frac{1}{2^{n+1}},$$

$$\frac{N_-}{N_++N_-}=\frac{1}{2}-\frac{1}{2^{n+1}}.$$

Hence the fraction of strips with upward (or downward) flux approaches $\frac{1}{2}$ exponentially fast in time. For $n\gg 1$ the number of upward and downward strips is nearly equal. The exponentially decreasing noncancellation, $(N_+-N_-)/(N_++N_-)=2^{-n}$, is, however, what leads to the growth of the total flux. This is because the number of strips grows faster (namely, as 4^n) than the rate of decrease of $(N_+-N_-)/(N_++N_-)$ (namely, 2^n). In general, if we pick a surface S and look at the "flux without cancellation," defined as

$$\tilde{\Phi}=\int_S|B_n|dS,$$

where B_n is the component of **B** normal to S, then we can quantify the effect of cancellation by a quantity γ_c, which gives the exponential rate of decrease of $\Phi/\tilde{\Phi}$,

$$\Phi/\tilde{\Phi}\sim\exp(-\gamma_c t).$$

Since $\Phi\sim\exp(\Gamma t)$ and $\tilde{\Phi}\sim\exp(\lambda_T t)$, we have $\Gamma=\lambda_T-\gamma_c$. Thus γ_c can be interpreted as the damping caused by the cancellation effect. If the cancellation effects are too strong, then, as shown in Ref. 16, it is possible to have chaotic flows in which magnetic fields damp (i.e., there is no fast dynamo). This corresponds to $\gamma_c>\lambda_T$. (In the example above $\lambda_T=T^{-1}\ln 4$, $\gamma_c=T^{-1}\ln 2$, $\Gamma=\lambda_T-\gamma_c=T^{-1}\ln 2$.)

It will also be of interest to calculate the fraction $P_{+,n}$ of the area in $0<(x,y)<1$, which has positive flux at time nT. Let $r=\alpha+\beta+\delta$ be the probability of a vector *not* flipping. For the present discussion, let us assume $r>\frac{1}{2}$. (The case $r<\frac{1}{2}$ is considered in Sec. IV E.) We obtain

$$P_{+,n}=rP_{+,n-1}+(1-r)(1-P_{+,n-1}).$$

For $P_{+,0}=1$, this gives

$$P_{+,n}=\tfrac{1}{2}+\tfrac{1}{2}(2r-1)^n.$$

[For uniform stretching, i.e., $\alpha=\beta=\gamma=\delta=\frac{1}{4}$ we have $r=\frac{3}{4}$, and $P_{+,n}$ is the same as $N_+/(N_++N_-)$.] Thus $P_{+,n}$ converges exponentially to $\frac{1}{2}$ as $\exp(-\nu n)$ with

$$\nu=-\ln(2r-1).$$

In comment (vi) at the end of Sec. III, we noted that chaotic flows *in two dimensions* do not produce dynamos. From the point of view of this section, the lack of dynamo action can be understood on the basis of the cancellation of flux. This is illustrated in Fig. 8, which shows a closed field line before [Fig. 8(a)] and after [Fig. 8(b)] stretching by a chaotic two-dimensional flow. The net flux crossing the reference dashed line has not increased. If, in such a two-dimensional situation, one examines the evolution of magnetic energy (instead of the flux through an area), one would find that it initially increases with time as a result of the exponential stretching of field lines. However, during this initial phase in which the magnetic energy increases, the spatial scale for variation of **B** decreases exponentially with time. When the spatial scale of **B** reaches the scale ξ at which resistivity becomes important, the field energy rapidly decays. To see how this occurs we note that the typical wavenumber κ increases exponentially with time, $\kappa\sim\exp(\gamma_\kappa t)$, with a corresponding diffusive damping time dependence $\sim\exp(-\int^t\kappa^2/R_m\,dt)$, where $\int^t\kappa^2\,dt\sim\gamma_\kappa^{-1}\exp(2\gamma_\kappa t)$. Thus the energy eventually damps very rapidly, roughly an exponential of an exponential, $\exp[-(\text{const})\times R_m^{-1}\exp(2\gamma_\kappa t)]$. (For an analytically worked out example where this type of scenario occurs see Refs. 6 and 8.)

We now offer some discussion on the possibility of a *steady* [i.e., $\mathbf{v}=\mathbf{v}(\mathbf{x})$ with no t dependence], fast dynamo with a smooth[14] flow. Numerical approaches to the question of whether such dynamos are possible are so far not conclusive.[9,12] The easiest way to show the possibility of a fast dynamo in a steady flow would be to find a steady chaotic flow

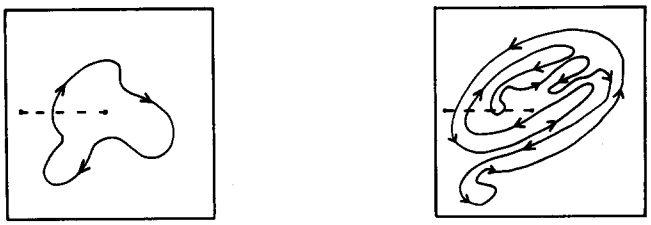

(a) (b)

FIG. 8. (a) An initial closed magnetic field line. (b) The same field line after stretching by a two-dimensional, chaotic flow. The flux through the dashed line does not grow exponentially, because of cancellation.

with *no* cancellation. Arnold *et al.*[8] demonstrate a concrete steady flow of this type (and with uniform stretching), but their example is in a space of negative geodesic curvature; thus it still remains unclear whether steady chaotic flows without cancellation are possible for real situations (in particular, in a Euclidean space). Bayly[15] *assumes* that such flows exist and derives some properties of the resulting steady fast dynamo. In particular, he shows that λ_L is a lower bound on the growth rate (this also follows from the discussion in Sec. IV B). The existence of a fast dynamo, however, does not *require* the total absence of fine-scale cancellation. This is clearly shown by our example in Figs. 6 and 7. [For the case of a two-dimensional flow, the cancellation is so exact that there is no dynamo (see Fig. 8).] The steady three-dimensional flow is, in a sense, intermediate between the two-dimensional map case and the three-dimensional map case: On the other hand, surfaces of section of steady three-dimensional flows yield two-dimensional maps (that is, pick a surface S and record the successive points on S that intersect the orbit). On the other hand, the magnetic field is not constrained to lie on the two-dimensional surface of section S. The latter consideration may be the more crucial. If it is, then exact cancellation (as occurs in the two-dimensional case) would not occur. Thus one would conclude that typical three-dimensional chaotic *steady* flows could yield fast dynamos and that these dynamos would exhibit a concentration of flux on a fractal (due to nonuniform stretching) as well as cancellation of flux on an arbitrarily fine scale.

E. Real part of frequency

All of the maps we have studied so far have the property of producing a field that is purely growing in time. Can the real part of the frequency be nonzero? This is certainly suggested by the fact that the operator in Eq. (1) is not self-adjoint. The two-strip baker map of Eq. (9) and Fig. 4 can be trivially modified to have a complex frequency by flipping both sections; then $\Phi_n = (-2)^n\Phi_0$. Also, the baker transformation of Eq. (10) (Fig. 7) can be modified to give a complex frequency. Take three sections, say, the α, γ, and δ sections, to be flipped. Then the flux satisfies $\Phi_{n+1} = -2\Phi_n$ or $\Phi_n = (-2)^n\Phi_0$, giving $\gamma = (\ln 2)/T$ and $\omega_r = \pi/T$. (For r, the probability of not flipping, less than $\frac{1}{2}$, $P_{+,n}$ has oscillatory decay.) Still, this class of baker transformations is special in the sense that the eigenfunction depends on x alone, whereas a vector $\mathbf{B}$ at $\mathbf{x} = (x,y)$ is flipped or not depending only on its value of y. For such maps it is easy to show that ω_r, the real part of ω, is either 0 or π, i.e., $\Phi_n \sim d^n$ with d a positive or negative real number.

To shed some light on the real part of ω for more general maps, we introduce another baker transformation,

$$\left.\begin{aligned} x_{n+1} &= \alpha x_n \\ y_{n+1} &= \alpha^{-1} y_n \end{aligned}\right\} \text{ if } y_n < \alpha,$$

$$\left.\begin{aligned} x_{n+1} &= \alpha + \beta(\xi - x_n) \\ y_{n+1} &= \beta^{-1}(1 - y_n) \end{aligned}\right\} \text{ if } y_n \geqslant \alpha \text{ and } x_n < \xi, \qquad (18)$$

$$\left.\begin{aligned} x_{n+1} &= \alpha + \beta x_n \\ y_{n+1} &= \beta^{-1}(y_n - \alpha) \end{aligned}\right\} \text{ if } y_n \geqslant \alpha \text{ and } x_n \geqslant \xi,$$

where $\beta = 1 - \alpha$ and $0 < \alpha, \xi < 1$; see Fig. 9. A vector at $\mathbf{x}$ can be reversed in direction by this map depending on x and y (i.e., $y \geqslant \alpha$, $x < \xi$), although the eigenfunction $\mathbf{B}(\mathbf{x})$ is of the form $B_y(x)\hat{e}_y$.

The special case of Eq. (18) with $\alpha = \xi$ can be simply analyzed because a part of the interval $x = 1$, $0 < y < \alpha$ is mapped onto the cut $y \geqslant \alpha$, $x = \xi$. If we define Φ_1 as the flux in $0 < x < \xi$ and Φ_2 as the flux in $\xi < x < 1$, we find (cf. Fig. 9)

$$\begin{pmatrix} \Phi_1 \\ \Phi_2 \end{pmatrix}_{n+1} = \mathbf{M} \begin{pmatrix} \Phi_1 \\ \Phi_2 \end{pmatrix}_n, \qquad (19)$$

where the matrix $\mathbf{M}$ is given by

$$\mathbf{M} = \begin{pmatrix} 1 & 1 \\ -1 & 1 \end{pmatrix} = \sqrt{2} \begin{pmatrix} \cos(\pi/4) & \sin(\pi/4) \\ -\sin(\pi/4) & \cos(\pi/4) \end{pmatrix}. \qquad (20)$$

This matrix has eigenvalues $\exp(\pm i\omega_r T + \gamma T)$, where $\omega_r T = \pi/4$, $\gamma T = (\ln 2)/2$. In fact, the total flux $\Phi = \Phi_1 + \Phi_2$ equals $2^{nT/2}\cos(nT\pi/4)$ for initial conditions $\Phi_1 = \alpha$, $\Phi_2 = 1 - \alpha$ [i.e., uniform $B_y(x)$]. Thus the flux grows and oscillates with a period $8T$. The fraction of area with positive flux can also be computed for $\xi = \alpha$. We find

$$P_{+,n} = \tfrac{1}{2}[1 + 2^{-nT/2}\cos(nT\pi/4)],$$

showing that $P_{+n} - \frac{1}{2}$ decays exponentially at a rate $\nu T = \ln\sqrt{2}$ and also has period $8T$.

Another special value of ξ for the map in Eq. (18) is $\xi = \alpha^2/[1 - \alpha(1 - \alpha)]$. For concreteness, let $\alpha = \frac{1}{2}$ and $\xi = \frac{1}{3}$. Let us define Φ_1 to be the flux for $0 \leqslant x < \frac{1}{3}$, Φ_2 the flux for $\frac{1}{3} \leqslant x < \frac{2}{3}$, and Φ_3 the flux for $\frac{2}{3} \leqslant x < 1$. After *two* iterations of the map, a portion of the segment $x = \frac{1}{3}$, $\frac{1}{2} < y < 1$ is mapped back upon the same cut. We find, as in Eq. (19),

$$\begin{pmatrix} \Phi_1 \\ \Phi_2 \\ \Phi_3 \end{pmatrix}_{n+1} = \mathbf{M} \begin{pmatrix} \Phi_1 \\ \Phi_2 \\ \Phi_3 \end{pmatrix}_n,$$

now with

$$\mathbf{M} = \begin{pmatrix} 1 & 1 & 0 \\ -1 & 0 & 1 \\ 0 & 1 & 1 \end{pmatrix}.$$

This matrix has eigenvalues $\lambda = 0$ and $\lambda = 1$, the latter repeated. The former eigenvalue represents infinite exponential decay. The latter corresponds to one stationary mode

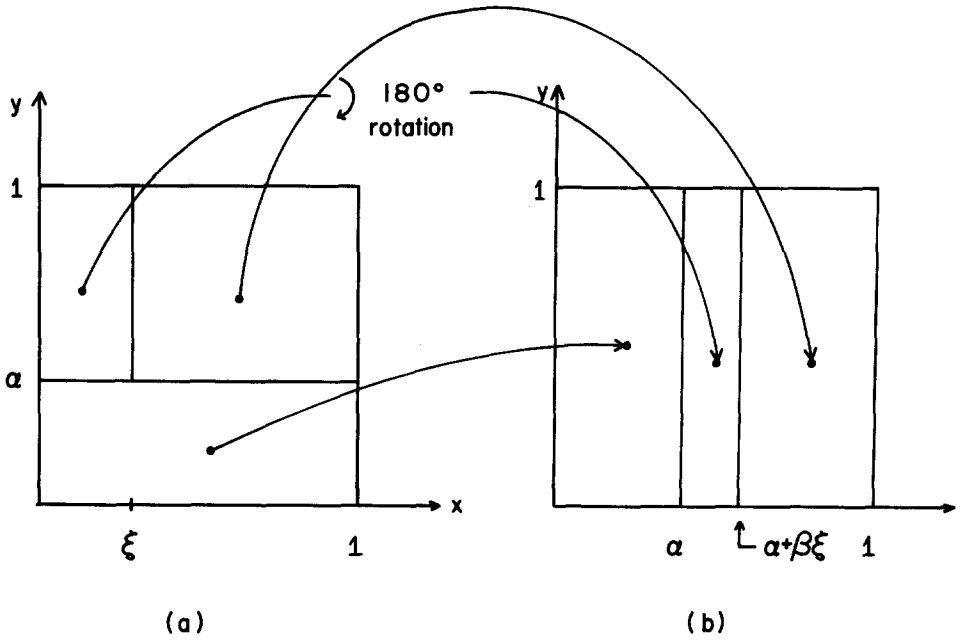

FIG. 9. Schematic illustrating Eq. (18), which is an example of a map yielding oscillatory growth.

and one mode that grows linearly rather than exponentially with respect to time.

The map (18) appears to be difficult to analyze for ξ other than $\xi = \alpha$ or $\xi = \alpha^2/[1-\alpha(1-\alpha)]$. More general results have been obtained numerically and are shown in Sec. V B. It is clear that the real part of ω in the example with $\xi = \alpha$ is due to vector cancellation, the subject of Sec. IV D.

In the above we have found that ω_r is commensurate with the map period, $(\omega_r T)/(2\pi) = \frac{1}{8}$. We can also exhibit examples where ω_r is incommensurate with the map period [i.e., the time variation is quasiperiodic and $(\omega_r T)/(2\pi)$ is an irrational number]. The examples constructed are a class of maps related to Eq. (18) for which Eq. (19) still holds but with the matrix M being of the form

$$\mathbf{M} = \begin{pmatrix} f & f \\ -g & h \end{pmatrix}, \tag{21}$$

where f, g, and h can be any integers. In this case $(\omega_r T)/(2\pi)$ can clearly be irrational [e.g., for $h = f = 1$ and $g = 2$ we have that $(\omega_r T)/(2\pi) = (\arctan\sqrt{2})/2\pi$, which is an irrational number]. The map yielding Eq. (21) is obtained as follows. We follow the procedure illustrated in Fig. 9 and take $\xi = \alpha$ as before. We then take each of the three strips in Fig. 9(b) and do further operations on them: we uniformly and incompressibly stretch each in y (by an amount f for the strip in $\alpha > x > 0$, by an amount g for the strip in $\alpha + \beta\xi > x > \alpha$, and by h for the strip in $1 > x > \alpha + \beta\xi$) and then place them back in the space they originally occupied. This is illustrated in Fig. 10 for the strip in $\alpha > x > 0$ ($f = 3$ in the figure).

For the baker's maps, Eqs. (9) and (10), we have specific time-periodic, three-dimensional flow models (Figs. 3 and 6) that do not cut field lines and which correspond to the map. This is not the case for the map (18) treated in this section. Thus we cannot definitely conclude that results obtained for the map (18) represent possible behavior for real dynamos resulting from time-periodic flows. Nevertheless, these results are suggestive. Concerning the possibility of a real frequency $(\omega_r T)/2\pi = 1/P$, where P is an integer, this

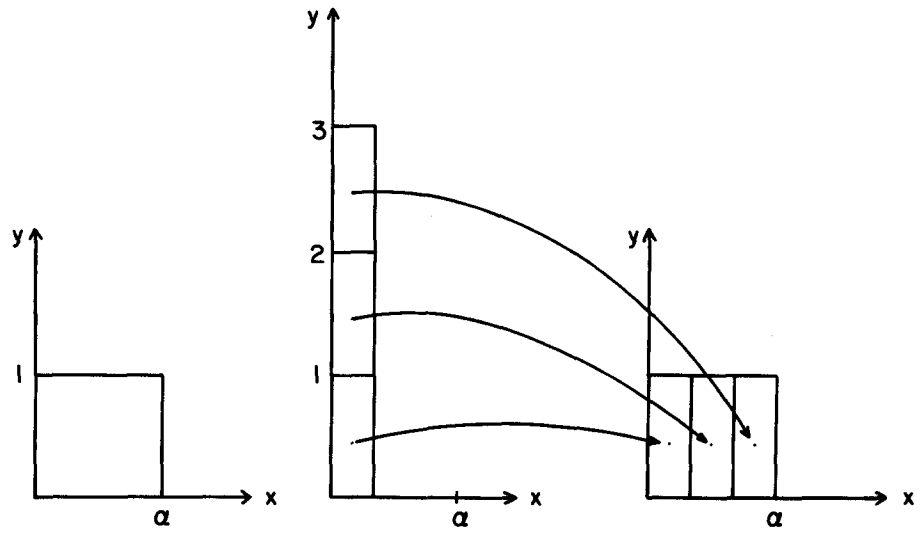

FIG. 10. Schematic illustrating the operation on the strip $\alpha > x > 0$ in Fig. 9(b) to yield Eq. (21).

can definitely occur by a mechanism other than that for (18). In particular, a three-dimensional map resulting from a three-dimensional time-periodic flow can be ergodic on a volume consisting of P disjoint subvolumes through which a chaotic orbit cycles successively through each region every P iterates. Thus if the initial magnetic field was nonzero in the first of these components and zero on the other $P-1$, on the first iterate the region of nonzero field would move to the second component, to the third on the next, to the fourth on the next, etc., and back to the first on the Pth iterate. Thus the field distribution can repeat every P iterates, yielding a frequency $(\omega_r T)/2\pi = 1/P$.

The tendency for the formation of fine scales (Sec. IV C), the tendency for a high degree of flux cancellation (Sec. IV D), and the possibility for real frequency (this subsection) pose inherent difficulties for numerical computations. A computational approach to calculating the zero resistivity flux growth rate is discussed next.

V. NUMERICAL RESULTS

In this section we first describe a numerical method constructed to study the fast dynamo problem in the limit $R_m \to \infty$ (Sec. V A). Our purpose is to use a code based on this method to investigate aspects of the dynamo problem discussed in Secs. II–IV (growth rate, real part of frequency, distribution of vector lengths, cancellation, and fractal structure). The special maps of Sec. IV were constructed explicitly in order to illustrate these features. We show results of our numerical procedure on these special maps in Sec. V B in order to illustrate the method, and to show how these features (specifically, distribution of vector lengths, cancellations, and cascade to shorter scales) create inherent difficulties. Then, in Sec. V C, we show the results of applying this method to more general maps. The results of Sec. V C suggest that the features encountered in the study of the idealized baker's map models of Sec. IV are to be expected in dynamos for typical unsteady three-dimensional chaotic flows.

A. Numerical method and qualitative features

Our numerical method takes advantage of the conjecture of Sec. III, namely, that the growth rate for $R_m \to \infty$ can be found by computing the exponentiation rate of increase of the flux through a fixed macroscopic area using the ideal $R_m = \infty$ equation, Eq. (2). Specifically, let us consider a map $\mathbf{x}_{n+1} = \mathbf{F}(\mathbf{x}_n)$ (for flows an analogous procedure applies), and denote the magnetic field at a location $\mathbf{x}$ and a time n by $\mathbf{B}(\mathbf{x},n)$ (in this section we set the time interval T between applications of the map to unity, $T=1$). We then choose a fixed surface S in $\mathbf{x}$ space and pick K points on this surface $\mathbf{x}^k$ ($k = 1,2,...,K$), where $\mathbf{x}^k$ can be chosen randomly with uniform distribution per unit area of S or from a grid. The flux through the surface S at time n is then approximately given by

$$\Phi_S(n) \cong \frac{A}{K}\sum_{k=1}^{K} \mathbf{B}(\mathbf{x}^k,n)\cdot\mathbf{N}(\mathbf{x}^k),$$

where $\mathbf{N}(\mathbf{x}^k)$ is the unit vector normal to the surface S at the point $\mathbf{x} = \mathbf{x}^k$ and A is the area of S. The problem then reduces to finding $\mathbf{B}$ at time n at the points $\mathbf{x}^k$ given an initial smooth magnetic field $\mathbf{B}(\mathbf{x},0)$. The calculation proceeds in two steps.

Step 1: We first determine for each $\mathbf{x}^k$ the corresponding initial value of $\mathbf{x}$ which when iterated forward n times under the map lands at the point $\mathbf{x}^k$. We denote this initial value $\mathbf{x}^k(n)$, and we obtain it by starting at $\mathbf{x}^k$ and iterating the map backward in time,

$$\mathbf{x}^k(n) = \mathbf{F}^{-n}(\mathbf{x}^k).$$

Note that

$$\mathbf{x}^k(n+1) = \mathbf{F}^{-1}[\mathbf{x}^k(n)],$$

so that, to find the initial conditions for calculating $\Phi_S(n)$ at successive later times, we can take the initial conditions for each $\mathbf{x}^k$ for the previous time and iterate them backward once.

Step 2: At each $\mathbf{x}^k(n)$ we evaluate $\mathbf{B}^k(n) = \mathbf{B}[\mathbf{x}^k(n),0]$ and iterate the magnetic field forward in time using the linearized map [the analog of Eq. (4)],

$$\mathbf{B}(\mathbf{x}^k,n) = \mathbf{B}^k(n)\cdot\{\nabla\mathbf{F}[\mathbf{x}^k(n)]\}\cdot\{\nabla\mathbf{F}[\mathbf{x}^k(n-1)]\} \cdot\cdots\cdot\{\nabla\mathbf{F}[\mathbf{x}^k(1)]\},$$

where $\nabla\mathbf{F}[\mathbf{x}^k(m)]$ denotes the Jacobian matrix of partial derivatives of $\mathbf{F}(\mathbf{x})$ evaluated at the position $\mathbf{x} = \mathbf{x}^k(m)$. For the vectors $\mathbf{x}^k(m)$ we use those already obtained numerically from the backward iteration in step 1 [and not orbits numerically calculated from forward iteration of $\mathbf{x}^k(n)$]. This ensures that the points $\mathbf{x}^k(0)$ lie on S with the initial distribution—either random or on a grid. This maneuver is necessary because machine roundoff is exacerbated by the exponential divergence of trajectories. (When applying the numerical technique to the two-dimensional baker's maps of Sec. IV, S is to be understood as a line segment, rather than a surface.)

For large n and chaotic orbits, the *direction* of $\mathbf{B}$ at time n and point $\mathbf{x}$ is typically primarily determined by the last few Jacobian matrix multiplications near time n. (This is because these preferentially amplify the vector component in the most unstable direction.) Thus the direction of $\mathbf{B}$ typically has a short range memory dependence on the orbit. Hence it does not "have time" to develop arbitrarily fine-scaled features. That is, the direction of $\mathbf{B}$ varies smoothly (see Greene[27] for a related discussion). In contrast, the sign and value of the field along this unstable direction clearly depend on the whole orbit and hence can become fine scaled. (Another way of phrasing this is to say that the magnitude and sign of $\mathbf{B}$ can vary on these decreasing length scales but $\mathbf{B}$ cannot *rotate* on such length scales.) Thus as n increases, for most of the positions $\mathbf{x}^k$, $\mathbf{B}$ becomes of the form

$$\mathbf{B}(\mathbf{x},n) \cong u(\mathbf{x},n)\mathbf{w}(\mathbf{x}),$$

where $\mathbf{w}(\mathbf{x})$ is smooth and $u(\mathbf{x},n)$ develops finer and finer scale dependence on $\mathbf{x}$ as n increases. Thus it is the variation of the scalar quantity $u(\mathbf{x},n)$ that is responsible for the tendency of flux to concentrate on a fractal and the tendency for cancellation. For the baker's models considered in Sec. IV, $\mathbf{w}(\mathbf{x})$ was a constant, namely, $\mathbf{y}_0$. The point here is that this is not much of a limitation. In particular, if we examine

$\mathbf{B}(\mathbf{x}^k,n)$ in some tiny enough region at large n, then $\mathbf{w}(\mathbf{x}^k)$ will be approximately constant in this region, while u is fine scaled; and the behavior, in this regard, is similar to that in the baker's models.[28]

Before presenting results produced by the numerical technique described above, we discuss the impact of some of the phenomena discussed in Sec. IV on the implementation of this (or any other) numerical method. In particular, we are concerned with the differential rate of stretching and the tendency for cancellation.

For the simple baker map of Eq. (9) and Fig. 4, in which there is no cancellation, we found that the fraction of the area contributing after n iterations to, say, 90% of the total flux through S scales as $(2\sqrt{\alpha\beta})^n$, where $\beta = 1-\alpha$. Thus for large n only a small number, k_*, of the K vectors on the surface S will be responsible for most of the flux, where

$$k_* \approx Q^n K, \tag{22}$$

with $Q = (2\sqrt{\alpha\beta})$. Note that $Q<1$ for $\alpha \neq \beta = 1-\alpha$. To have a reliable computation of the mean vector length, k_* must be large. For $\alpha = \beta = \frac{1}{2}$, Q is unity, and all vectors contribute to the sum. (This is the trivial case in which all vectors have the same length.) Notice that Eq. (22) indicates that (except when $\alpha = \beta = \frac{1}{2}$) k_* decreases exponentially with n and will therefore eventually become too small for reliable computation of the flux. Also note that this problem is more severe for smaller α, i.e., for wider distribution of vector stretching amplitudes. For example, taking $K = 10^4$, and assuming we require $k_* \gtrsim 10^3$ for good statistics, we see that the results will be reliable for $n \lesssim 100$ for $\alpha = 0.4$ ($Q = 0.98$ and ratio of maximum to minimum stretch $\beta/\alpha = 1.5$), but $n \lesssim 10$ is required for $\alpha = 0.2$ ($Q = 0.8$ and $\beta/\alpha = 4$). As we have discussed in Sec. IV, we expect general maps (and flows) to have nonuniform stretching.

Generally, we are limited in K by computer time. [Storage is not an issue because the different orbits $\mathbf{x}^k(n)$ are independent of each other. This is a major advantage of our numerical scheme compared, say, to a Eulerian integration of (1).] This generally means that for reasonable distribution of stretch (corresponding to $\beta/\alpha \leqslant 3$), accurate exponentiation rates of magnetic flux can be computed. However, for a very wide distribution, it may not be possible to produce even several e-foldings before accuracy is lost.

The second issue, cancellation, is illustrated by the four-slice $\alpha, \beta, \gamma, \delta$ baker transformation of Eq. (10) and Fig. 7. It is convenient for discussion to pick $\alpha = \beta = \gamma = \delta = \frac{1}{4}$ initially, so that no differential stretching effects enter. An important measure of the effect of cancellation on the numerical method is the quantity $P_{+,n}$ determined in Sec. IV D, which is equal to the probability of a point $\mathbf{x}^k$ having positive field, $B_y^k > 0$, at step n (assuming uniform upward field at time $n = 0$). Let f_n be the actual fraction of the K points on S that have positive field at step n. In a numerical computation with K orbits the computation of the flux Φ_S will be accurate as long as $|P_{+,n} - \frac{1}{2}| \gg 1/K^{1/2}$. After that point, statistical fluctuations of f_n with amplitude $1/\sqrt{K}$, cause the effect of cancellations on the growth rate to be computed inaccurately. The above discussion can easily be generalized to the situation in which differential stretching occurs. In this case, the same arguments apply but with K replaced by k_*. Thus the condition for accurate computation of the flux is $|P_{+,n} - \frac{1}{2}| \gg 1/\sqrt{k_*} \approx Q^{-n/2}/\sqrt{K}$.

B. Results: Baker transformations

In this subsection we present and discuss the results of applying our numerical scheme to the various baker transformations introduced in Sec. IV. Our purpose is to illustrate further the effects of distribution of stretching and cancellation and to aid in interpreting the results of applying the numerical method to more general maps.

In Fig. 11 we show results for the flux for the first baker map, of Eq. (9) and Fig. 4, i.e., without flipping, with $\alpha = 0.3$, and $K = 5000$. The Lyapunov exponent, averaged over all the particles, equals 0.611, for $n \gtrsim 4$, in agreement with Eq. (11) which gives $\lambda_L = 0.6109$. (Again, $T = 1$.) The standard deviation of the distribution of Lyapunov exponent behaves as $1/\sqrt{n}$, as expected. The exponentiation rate of the flux is computed to be 0.68 for $n \lesssim 100$, in agreement with $\Gamma = \lambda_T = \ln 2 = 0.693\ldots$. This computation is not accurate for $n > 100$. For $\alpha = 0.3$, we obtain $k_* = 64$ for $n = 50$ and $k_* = 7$ for $n = 75$, so the deterioration in Γ for $n \gtrsim 100$ is expected.

In Fig. 12 we show numerical results on the four-strip baker transformation with flipping in the third (γ) section, i.e., the map of Eq. (10) and Fig. 7. We pick $\alpha = \frac{1}{3}$ and $\beta = \gamma = \delta = \frac{2}{3}$ so that there will be differential stretching ($\alpha/\beta = \frac{1}{2}$) as well as cancellation. The Lyapunov exponent averaged over all orbits for $n \gtrsim 5$ is computed to be $\lambda_L = 1.37$, which agrees well with Eq. (12), which gives $\lambda_L = \alpha \ln(1/\alpha) + 3\beta \ln(1/\beta) = 1.369$. Also, the distribution function of Lyapunov exponents has a standard deviation that decreases as $1/\sqrt{n}$, as expected. Figure 12(a) shows the flux without cancellation

$$\tilde{\Phi}_n = \int_S |\mathbf{B}\cdot\mathbf{N}|\,dS \approx \frac{A}{K}\sum_{k=1}^{K} |\mathbf{B}^k\cdot\mathbf{N}^k| \tag{23}$$

as a function of n. In Eq. (23) A is the length of the line S in the two-dimensional case and the area of the surface S in the three-dimensional case. The exponentiation rate of this quantity is expected to be equal to the topological entropy. Numerically, we find for this rate 1.39, which is in excellent

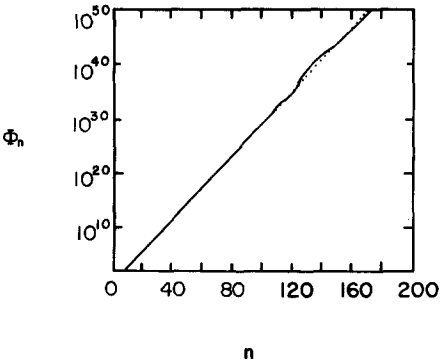

FIG. 11. Flux as a function of iteration number for the two-strip baker's map [Eq. (9)] with $\alpha = 0.3$.

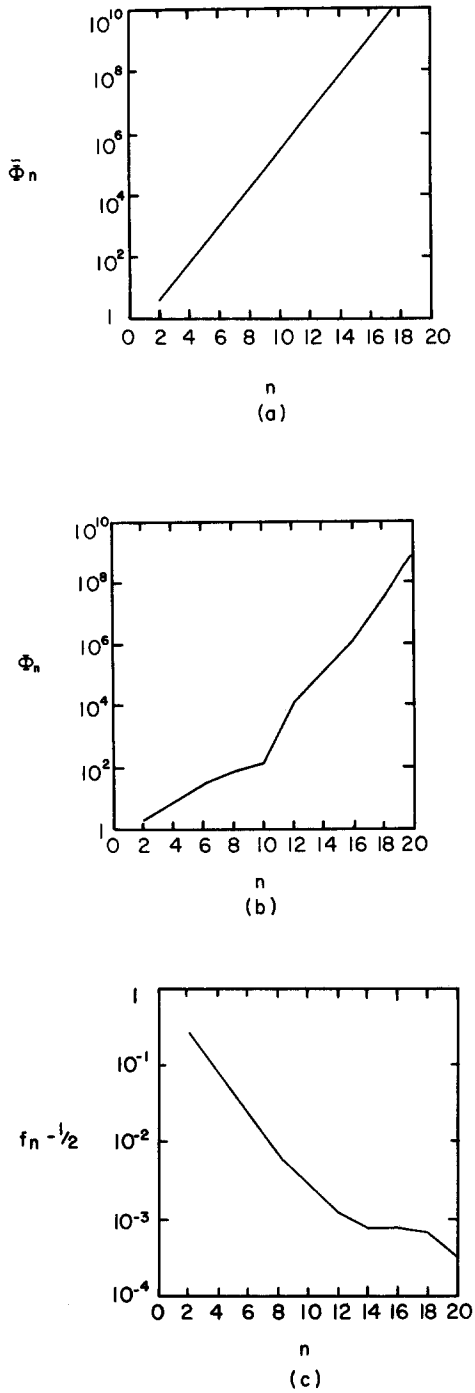

FIG. 12. Results for the four-strip baker's map Eq. (10): (a) $\tilde{\Phi}_n$, the flux without cancellation, Eq. (23); (b) the flux Φ_n; and (c) $f_n - \frac{1}{2}$.

agreement with its expected value of $\lambda_T = \ln 4 = 1.386\ldots$. The number of orbits used was $K = 10^5$. Also, the distribution of stretching was modest ($\lambda_T/\lambda_L = 1.01$), so that the arguments of the previous section indicate that the topological entropy should be computed accurately even for much larger n. In fact, using the results of Appendix C ($\alpha = \frac{1}{3}$ and $\beta = \frac{2}{3}$ yield $Q = 0.9837$), we find that for $K = 10^5$ the topological entropy computation (i.e., the computation of the exponential rate of increase of $\tilde{\Phi}_n$) should be accurate for $n \lesssim 300$ (to obtain this we required $k_* \approx KQ^n > 10^3$). Figure 12(b) shows the total flux Φ_n as a function of n, and Fig. 12(c) shows $f_n - \frac{1}{2}$, where f_n is the fraction of points $\mathbf{x}^k$ with $B_y^k > 0$. For $n \gtrsim 10$, we obtain an exponentiation rate $\Gamma = 0.67$, in reasonable agreement with the expected value $\ln 2 = 0.693\ldots$. For $n \gtrsim 10$, the exponentiation rate is not very constant but is of order $\lambda_T = \ln 4$. Also, $f_n - \frac{1}{2}$ has exponentiation decay rate $\nu = 0.61$ for $n \lesssim 10$. From Sec. IV D, the expected value is $\nu = -\ln(2r-1)$, with $r = \frac{7}{9}$, or $\nu = 0.588\ldots$. For $n \gtrsim 10$, $f_n - \frac{1}{2}$ exhibits statistical fluctuations with level consistent with $1/\sqrt{K} \sim 1/\sqrt{k_*} \sim 3 \times 10^{-3}$. Notice that the point at which the exponential decay of $f_n - \frac{1}{2}$ ceases to mask the statistical fluctuations ($n \sim 10$) agrees well with the point where the flux begins to exponentiate at a rate closer to the topological entropy.

In Sec. IV E we introduced the map (18) (Fig. 9) to illustrate the possibility of a real part of the frequency. The case $\alpha = \xi = \frac{1}{2}$, with $K = 10^3$ particles, is shown in Fig. 13. From the results of Fig. 13(a) we compute the growth rate to be $\Gamma = 0.346$, which is in good agreement with the expected value $\ln\sqrt{2} = 0.346\ldots$. Also, the period 8 ($\omega_r = \pi/4$) is evident. The cancellation factor $f_n - \frac{1}{2}$ is shown in Fig. 13(b). The damping rate is computed to be $\nu = 0.34$, also in

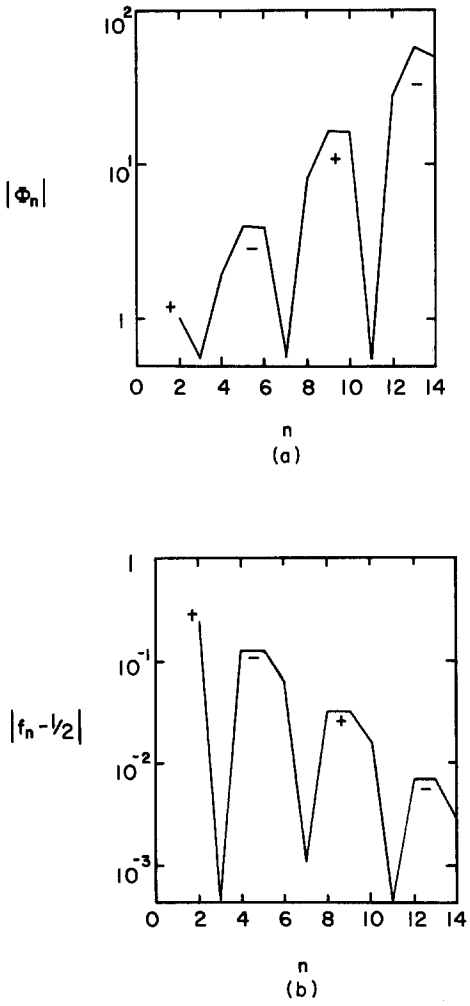

FIG. 13. Results for the map Eq. (18) with $\alpha = \xi = \frac{1}{2}$: (a) the flux $|\Phi_n|$, and (b) $|f_n - \frac{1}{2}|$. The $\pm$ signs again indicate the sign of Φ_n and $f_n - \frac{1}{2}$.

agreement with $\ln \sqrt{2} = 0.346...$, as discussed in Sec. IV E. Again, period 8 is evident. This case is particularly tractable numerically because all vectors stretch by the same factor, namely, 2. Therefore the Lyapunov exponent and the topological entropy both equal ln 2. The effect of cancellation is to reduce the growth rate and provide ω_r. Also, the flux Φ_n and the cancellation factor $f_n - \frac{1}{2}$ are accurate as long as $f_n - \frac{1}{2} > 1/\sqrt{K} \simeq 3 \times 10^{-2}$ or $n \lesssim 12$ as expected.

In Fig. 14 we show results for the same map [Eq. (18)] but with $\alpha = 0.5$, $\xi = 0.4$. The number of orbits used was $K = 10^5$. Since $\alpha = \beta = \frac{1}{2}$, $Q \equiv 2\sqrt{\alpha\beta}$ equals unity and $k_* = K$. The flux Φ_n and the fraction $f_n - \frac{1}{2}$ are shown in Figs. 14(a) and 14(b), respectively, showing growth and oscillation. We measure $\omega_r \cong 0.37$ (period $\cong 17$) and $\gamma \cong 0.24$. The topological entropy λ_T and the Lyapunov exponent λ_L are measured to be 0.693. This value is in agreement with the theoretical value ln 2 for both (equal because $\alpha = \beta$). The decay rate of $f_n - \frac{1}{2}$ is $\nu = 0.45$, also with period 17. Note that $\nu + \gamma \simeq \lambda_T$. This result is to be expected because of the uniform rate of stretching, i.e., $\alpha = \beta$. As before, the results are expected not to be degraded by cancellation as long as $|f_n - \frac{1}{2}| > 1/\sqrt{k_*} = 3 \times 10^{-3}$; that is, for $n \lesssim 12$. The behavior of Φ_n and of $f_n - \frac{1}{2}$ is indeed observed to deviate from (complex) exponential behavior beyond this point.

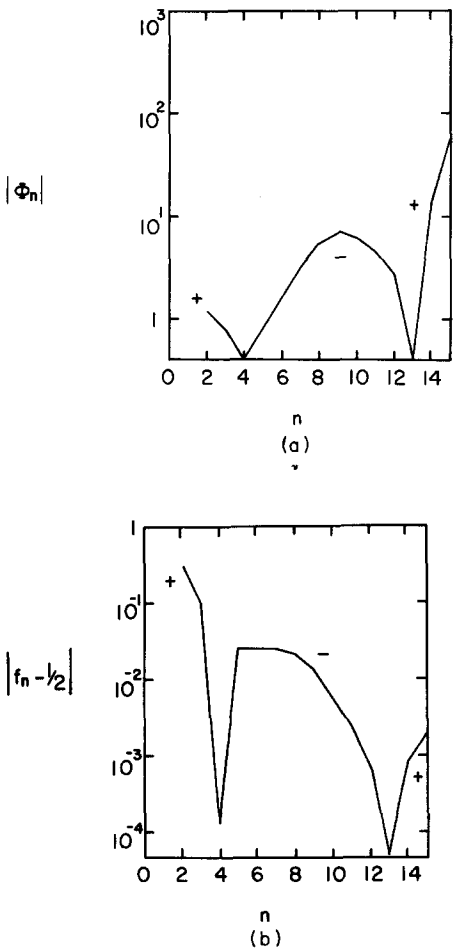

FIG. 14. Results for the map Eq. (18) with $\alpha = 0.5$ and $\xi = 0.4$: (a) the flux $|\Phi_n|$, and (b) $|f_n - \frac{1}{2}|$. The signs again indicate the sign of Φ_n and $f_n - \frac{1}{2}$.

C. Results: *ABC* maps

In this section we present the results of applying our numerical scheme to a class of continuous three-dimensional maps. It is to be expected that the properties of these maps are typical of what happens in unsteady, three-dimensional chaotic flows; in contrast, one may question this for the maps of Sec. IV, which were artificially constructed to exhibit certain properties of the dynamo process. In particular, the stretch–twist–fold process, on which Sec. IV is based, implies that $\mathbf{v}(\mathbf{x},t)$ is not continuous in $\mathbf{x}$. To see this, we note that there are points on the surface of the figure-eight shaped tube in Fig. 2(c) that are separated before the fold but coincide after the fold [Fig. 2(d)]. In this section we consider cases with spatially continuous velocity. The class of maps we consider is related to certain divergence-free flows having the property $\partial v_x/\partial x = \partial v_y/\partial y = \partial v_z/\partial z = 0$.

A numerical scheme for integrating the streamlines of such flows [i.e., Eq. (3)] is

$$x_{n+1} = x_n + T v_x(y_n, z_n),$$
$$y_{n+1} = y_n + T v_y(x_{n+1}, z_n), \tag{24}$$
$$z_{n+1} = z_n + T v_z(x_{n+1}, y_{n+1}),$$

where T is a constant. This numerical scheme is stable for arbitrary T because of its semi-implicit nature. In particular, the determinant of the Jacobian matrix of $(x_{n+1}, y_{n+1}, z_{n+1})$ with respect to (x_n, y_n, z_n) is exactly unity, i.e., the map (24) is exactly volume preserving. We will generally deal with these maps with relatively large values of T. This allows much faster computations. Another major reason for this is that for small T [i.e., when (24) approximates well steady flows given by the solution of the differential equation, $d\mathbf{x}/dt = \mathbf{v}(\mathbf{x}) = \mathbf{x}_0 v_x(y,z) + \mathbf{y}_0 v_y(x,z) + \mathbf{z}_0 v_z(x,y)$] the chaotic region of space may be quite small. For example, the region of chaotic streamlines for the steady flows called *ABC* flows,[29-31]

$$v_x = A \sin z + C \cos y,$$
$$v_y = B \sin x + A \cos z, \tag{25}$$
$$v_z = C \sin y + B \cos x,$$

is a rather small fraction of the cube of periodicity[31] (having sides of length 2π). On the other hand, we find that for $A \sim B \sim C \sim T \sim 1$, the map (24) based upon the *ABC* flow has a chaotic region that extends throughout almost all space. (This is related to the two-dimensional case in which the "leapfrog" scheme for the pendulum $dq/dt = p$, $dp/dt = -\sin q$, i.e., $q_{n+1} = q_n + T p_n$, $p_{n+1} = p_n - T \sin q_{n+1}$, is the Taylor–Chirikov standard map. The pendulum is of course integrable, but the standard map has large chaotic regions for $T \gtrsim 1$.) Also, we note that the map (24) results *exactly* for a time-periodic flow with velocity given by

$$\mathbf{v}(\mathbf{x},t) = \hat{v}_x(y,z)\mathbf{x}_0 \sum_{n=-\infty}^{+\infty} \delta(t-nT)$$
$$+ \hat{v}_y(x,z)\mathbf{y}_0 \sum_{n=-\infty}^{+\infty} \delta(t-nT-\epsilon)$$
$$+ \hat{v}_z(x,y)\mathbf{z}_0 \sum_{n=-\infty}^{+\infty} \delta(t-nT-2\epsilon)$$

(where ϵ denotes a small positive quantity), after integrating $d\mathbf{x}/dt = \mathbf{v}$ through the delta functions at $t = nT$, $nT + \epsilon$, $nT + 2\epsilon$. More generally, time-periodic flows (including those which are continuous in time) result in three-dimensional volume preserving maps when snapshots are taken at $t = nT$, and Eqs. (24) and (25) should yield features that are typical of these.

In Fig. 15 we show the results of applying our numerical method to the *ABC* map[32] (24), (25), with $A = B = C = 1$, and $T = 1.5$, with $K = 2.5\times 10^6$ orbits. The Lyapunov exponent is computed to be 0.75, and from Fig. 15(a) (i.e., the flux without cancellation), the topological entropy is equal to 0.97. In Fig. 15(b) we see evidence of oscillation in Φ_n for $n \lesssim 10$. These results are consistent with the possibility of two unstable modes, one with $\gamma = 0.70$ and $\omega_r = 0$, and another with γ about 10% lower but with $\omega_r \simeq 1.2$ (period $\simeq 5$). The fraction $f_n - \frac{1}{2}$ displayed in Fig. 15(c) shows a decay rate $\nu \simeq 0.30$ and a period of about 5. This is consistent with the picture of two unstable modes: the faster growing mode dominates in flux (for $n \gtrsim 10$) but does not dominate the slower growing mode in $f_n - \frac{1}{2}$ because the length scales of the latter evidently do not decrease as rapidly. That is, the flux of the faster growing mode concentrates onto a smaller area as it grows, but $f_n - \frac{1}{2}$ is not influenced because it is unrelated to the distribution of vector lengths. For $K = 2.5\times 10^6$, we estimate k_* to be 10^5 at $n = 15$, so that the statistical level $1/\sqrt{k_*}$ is 3×10^{-3}. The fact that $|f_n - \frac{1}{2}|$ is greater than this quantity over the whole range indicates that the results are accurate over that range. In fact, the results shown in Fig. 15 agree with those of another run with fewer orbits whenever the inequality $|f_n - \frac{1}{2}| > 1/\sqrt{k_*}$ is satisfied for the latter run.

In Fig. 16 we show the results of another case with the *ABC* map of Eqs. (24) and (25), with $A = 1$, $B = \sqrt{\frac{2}{3}}$, $C = \sqrt{\frac{1}{3}}$, as in Refs. 12 and 31, and with $T = 3$ and $K = 10^5$. The Lyapunov exponent is $\lambda = 1.49$ and the topological entropy, from Fig. 16(a), is $\lambda_T = 1.83$. The flux, from Fig. 16(b), has growth rate $\gamma = 0.9$ (with no observable value of ω_r) for $n \lesssim 8$. Thereafter, the flux grows irregularly, but with an average growth rate near the topological entropy. The fraction of orbits with $B_n > 0$, $f_n - \frac{1}{2}$ is shown in Fig. 16(c). Its decay rate ν is 0.8. The results of this case are qualitatively very similar to those of the four-strip baker map with cancellation shown in Fig. 12.

The fractal nature of the magnetic field produced is shown clearly in Fig. 17. The parameters are those of Fig. 15 and the surface S is $0.8 \leqslant (x,y) \leqslant 1.2$ and $z = 1$. We have plotted only those points on a 100×100 grid whose field contributes to 90% of the total flux without cancellation $\tilde{\Phi}_n$. That is, starting with the vectors with the largest value of $|B_z|$, we mark their position on the surface S and continue until the sum of $|B_z|A/K$, where A is the area of S, equals 0.9 of the value obtained for the sum of $|B_z|A/K$ for all 10 000 points in the grid. The points with positive B_z and with negative B_z are plotted as plus and minus signs, respectively. The general structure set up at $n = 3$, has little variation along lines having $\delta y/\delta x \simeq 1.4$, the direction associated with the maximum Lyapunov exponent, projected on the plane $z = 1$. The maximum variation is along lines having $\delta y/\delta x \simeq -0.7$. As n increases, two phenomena occur. First, successive strips elongated in the maximum Lyapunov direction are removed, much in the manner that the familiar Cantor set is formed. Second, some strips with $B_z < 0$ are placed in areas previously having $B_z > 0$ and vice versa. The tendency for fine-scale structure to form with increasing n is clearly evi-

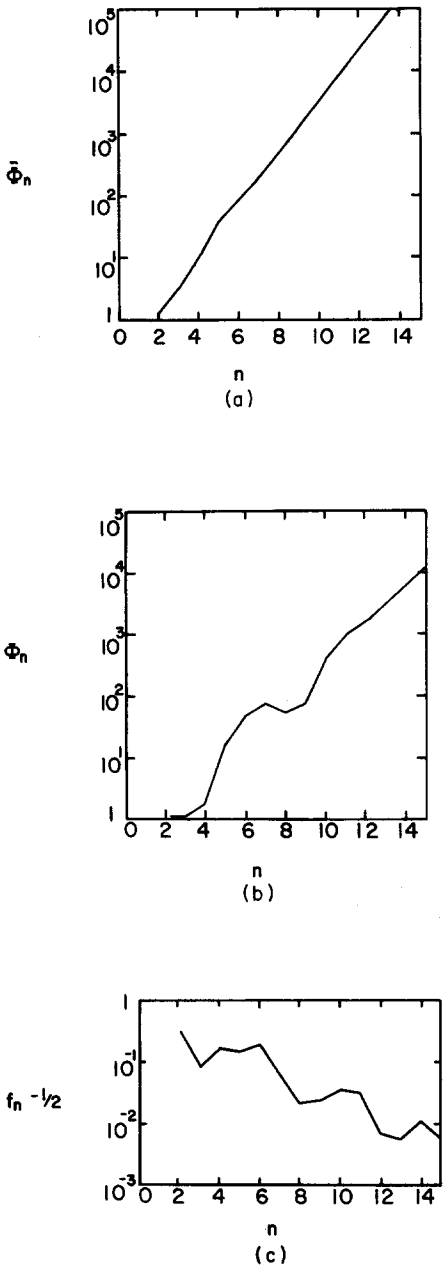

FIG. 15. Results for the *ABC* map with $A = B = C = 1$ and $T = 1.5$: (a) $\tilde{\Phi}_n$, (b) Φ_n, and (c) $f_n - \frac{1}{2}$.

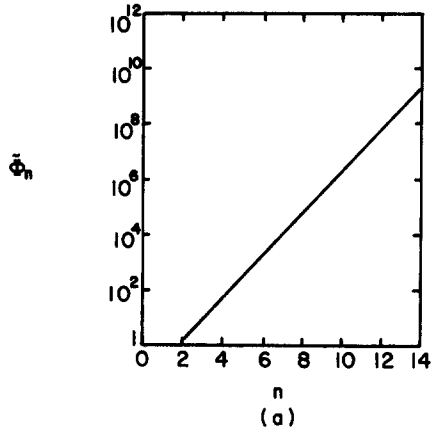

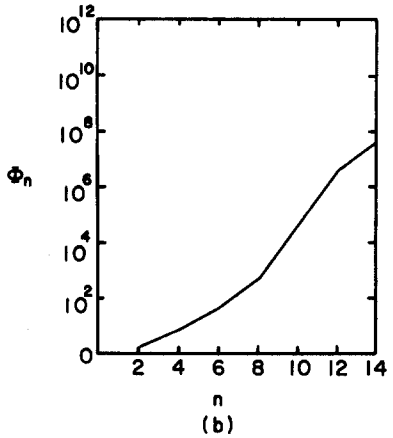

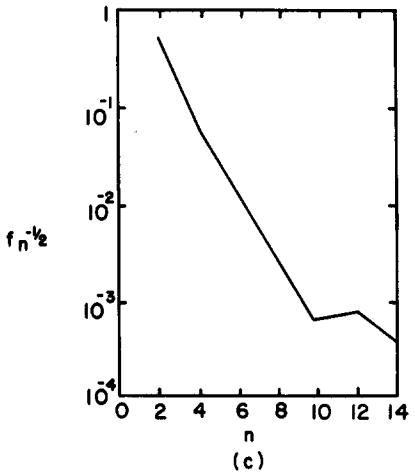

FIG. 16. Results for the *ABC* map with $A = 1$, $B = \sqrt{\frac{2}{3}}$, $C = \sqrt{\frac{1}{3}}$, and $T = 3$: (a) $\bar{\Phi}_n$, (b) Φ_n, and (c) $|f_n - \frac{1}{2}|$.

dent. Also, the fraction of vectors in the grid that contribute to 90% of the flux without cancellation is seen to decrease with n. Hence the field becomes more and more spatially intermittent, again indicating the tendency for the flux to concentrate on a fractal.

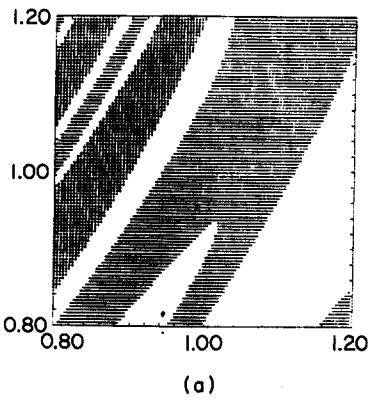

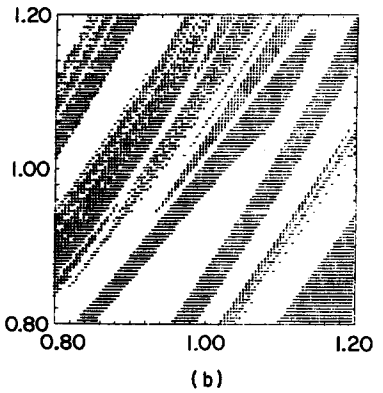

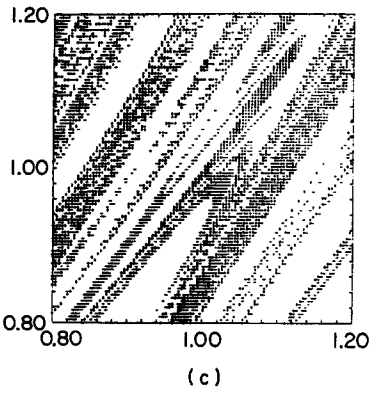

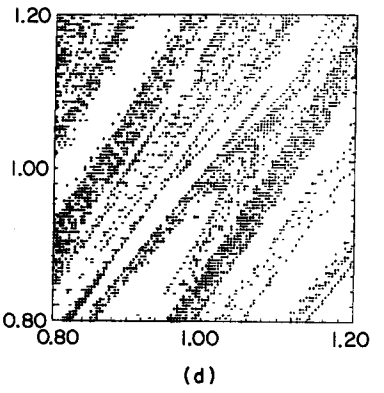

FIG. 17. Location of points in a 100×100 grid whose field contributes to 90% of $\bar{\Phi}_n$ at (a) $n = 3$, (b) $n = 5$, (c) $n = 7$, and (d) $n = 9$. Points with $B_z > 0$ are plotted as a plus sign, and points with $B_z < 0$ are plotted as a minus sign. Parameters are those for Fig. 15 and the surface examined is located at $z = 1$ and $0.8 < (x,y) < 1.2$.

VI. CONCLUSIONS

Using simple idealized models it has been argued that fast kinematic dynamos can occur for typical unsteady, three-dimensional, chaotic flows, and that, in the $R_m \to \infty$ limit, they typically have the following properties.

(a) The magnetic flux concentrates on a fractal set, i.e., exhibits spatial intermittency, because of the distribution of vector stretching. Another effect of the distribution of vector lengths, which is expected in general to be approximately lognormal, is that the growth rate can be larger than the Lyapunov exponent. The growth rate is in general limited by the topological entropy.

(b) The magnetic field vector rapidly oscillates between parallel and antiparallel directions. This rapid oscillation leads to a flux cancellation that is exponential with respect to time, and which can lead to a reduction in growth rate relative to the topological entropy. [As shown in Ref. 16, this reduction can lead to negative growth rate (damping).] Without cancellation the growth rate equals the topological entropy.

(c) Oscillatory unstable modes may occur.

The simple models we have employed illustrate quantitatively the relationship between the stretching and cancellation on the one hand, and the dynamo properties (i.e., the fractal nature of the magnetic field and its dimension, the growth rate, and the real part of ω) on the other. Furthermore, using a numerical technique for investigating the $R_m \to \infty$ limit, these results have been shown to hold for a more representative example, the *ABC* map.[33]

ACKNOWLEDGMENTS

We wish to acknowledge useful conversations with T. M. Antonsen, A. N. Kaufman, S. Newhouse, and H. Strauss.

This work was supported by the U.S. Department of Energy, the Office of Naval Research, and NASA.

APPENDIX A: LACK OF DYNAMO ACTIVITY IN A CLASS OF THREE-DIMENSIONAL CHAOTIC FLOWS

Our purpose in this appendix is to exhibit a class of flows, with v_z a constant, that do not exhibit dynamo activity in spite of having chaotic orbits. We also discuss some properties of such flows. Specifically, we discuss how the zero dynamo growth rate of such flows is due to perfect cancellation of the form described in Sec. IV D, and yields flow-aligned fields $\mathbf{B} = \alpha \mathbf{v}$.

In this appendix we consider flows of the form

$$\mathbf{v} = \nabla\phi(x,y,z) \times \mathbf{z}_0 + v_0 \mathbf{z}_0. \tag{A1}$$

In comment (vi) at the end of Sec. III we showed that this flow can be chaotic. We now show that it cannot produce a dynamo. This proof, which is a generalization of the Cowling theorem,[6] is based upon a discussion with Strauss. The z component of Eq. (1) gives

$$\frac{dB_z}{dt} = \frac{\partial B_z}{\partial t} + \mathbf{v}\cdot\nabla B_z = \frac{1}{R_m}\nabla^2 B_z. \tag{A2}$$

Thus B_z approaches a constant B_0 as $t \to \infty$. For appropriate boundary conditions B_0 is the average of the initial value B_z. For large R_m and chaotic flow this occurs on a time scale much faster than R_m because the convection term mixes B_z into long thin sheets. Then the diffusion term diffuses B_z across these sheets, as soon as the scale length approaches $R_m^{-1/2}$. For B_z uniform, the magnetic field can also be written in the form (A1), $\mathbf{B} = \nabla\psi(x,y,z) \times \mathbf{z}_0 + B_0 \mathbf{z}_0$. The z component of Ohm's law

$$\frac{\partial \mathbf{A}}{\partial t} = \mathbf{v} \times \mathbf{B} - \nabla\mu + R_m^{-1/2}\nabla^2 \mathbf{A},$$

with $\mathbf{A} = \psi \mathbf{z}_0 + B_0 r \boldsymbol{\theta}_0/2$, is

$$\frac{\partial \psi}{\partial t} + \mathbf{v}_\perp \cdot \nabla\psi = -\frac{\partial \mu}{\partial z} + \frac{1}{R_m}\nabla^2\psi \tag{A3a}$$

or

$$\frac{d\psi}{dt} = \frac{\partial}{\partial z}(v_0\psi - \mu) + \frac{1}{R_m}\nabla^2\psi. \tag{A3b}$$

The other components of Ohm's law produce ($\nabla_\perp \equiv \nabla - \mathbf{z}_0 \partial/\partial z$)

$$\nabla_\perp(\mu + B_0\phi - v_0\psi) = 0$$

or $\mu = v_0\psi - B_0\phi + g(z)$. But $g(z)$ can be removed by a gauge transformation (changing only $\psi = A_z$). Using this and $d\phi/dt = v_0\, \partial\phi/\partial z$, we obtain from Eq. (A3)

$$\frac{d\bar{\psi}}{dt} - \frac{1}{R_m}\nabla^2\bar{\psi} = \frac{B_0}{R_m}\nabla^2\phi, \tag{A4}$$

where $\bar{\psi} = v_0\psi - B_0\phi$. This is a linear equation for $\bar{\psi}$ in which the term $f(\mathbf{x}) \equiv (B_0/R_m)\nabla^2\phi$ acts as a source. With appropriate boundary conditions, the homogeneous solution $\bar{\psi}_h$ decays to a constant, as for Eq. (A2). Thus with the source present, the solution $\bar{\psi}$ is of the form $\bar{\psi} = \bar{\psi}_h(\mathbf{x},t) + t\langle f\rangle + \bar{\psi}_1(\mathbf{x})$, where $\langle f\rangle$ is the volume average of f and $\bar{\psi}_1$ satisfies $\mathbf{v}\cdot\nabla\bar{\psi}_1 - R_m^{-1}\nabla^2\bar{\psi}_1 = f - \langle f\rangle$. The mean value of the left side of the equation for $\bar{\psi}_1$ can be guaranteed to be zero by the boundary conditions. The $t\langle f\rangle$ term does not contribute to $\mathbf{B}_\perp = \nabla\psi \times \mathbf{z}_0$. Thus $\mathbf{B}_\perp$ relaxes to a *steady* spatially varying field with magnitude proportional to B_0, the *initial* spatially averaged B_z. Hence there is no dynamo (amplification of initial field).

For large R_m the $\nabla^2\phi$ term in Eq. (A4) is negligible because ϕ does not have the short scale lengths that $\bar{\psi}$ develops due to convection. Thus $\bar{\psi}$ convects as a passive scalar and, for chaotic flows, becomes a constant, $\psi = B_0\phi/v_0 + (\text{const})$. This implies that for large R_m the full magnetic field relaxes to the state

$$\mathbf{B} = \alpha \mathbf{v}, \tag{A5}$$

where $\alpha = B_0/v_0$ is a constant. Such flow-aligned fields clearly satisfy $\partial\mathbf{B}/\partial t = \nabla \times (\mathbf{v} \times \mathbf{B}) = 0$. Again $\mathbf{B} \sim \mathbf{B}_0$ so there is no dynamo. As discussed in Sec. IV D, the growth rate is zero because of cancellation of flux.

The condition (A5) can be obtained independently by requiring steady state $\mathbf{E} = -\nabla\Phi = -\mathbf{v} \times \mathbf{B}$. The equation

$$\mathbf{v}\cdot\nabla\Phi = 0 \tag{A6}$$

implies that Φ is a constant on the region covered by the chaotic orbit. From this it follows that the magnetic field is flow aligned, $\mathbf{B} = \alpha(\mathbf{x})\mathbf{v}$. From $\nabla\cdot\mathbf{B} = \nabla\cdot\mathbf{v} = 0$ we find

$$\mathbf{v}\cdot\nabla\alpha = 0, \tag{A7}$$

implying that α also is a constant on the region covered by the ergodic orbit. Both the potential Φ and α are constants because no streamfunction A (with $\mathbf{v}\cdot\nabla A = 0$) exists. For an integrable flow of this class, i.e., with $\partial\phi/\partial z = 0$ and for $\mathbf{E} = 0$, we obtain in steady state

$$\mathbf{B} = \alpha(\phi)\mathbf{v}, \tag{A8}$$

representing the tendency for $\mathbf{B}$ to line up with the streamlines because of differential flow. No fast dynamo is possible for such flows because there is no positive Lyapunov exponent.

APPENDIX B: FURTHER DISCUSSION OF FRACTAL DIMENSION FOR THE MAP GIVEN BY EQ. (9)

To discuss concepts of fractal dimension further, let $\Phi_n(a,b)$ be the upward flux through an interval $a \leqslant x \leqslant b$ at time nT. Since the total flux doubles on every iterate $[\Phi_n(0,1) = 2^n\Phi_0(0,1)]$, we normalize Φ_n as follows:

$$\mu_n(a,b) = \Phi_n(a,b)/[2^n\Phi_0(0,1)].$$

Assuming the y component of the magnetic field at $n = 0$ is positive everywhere, we have for Eq. (9) that $\mu_n(0,x)$ is a positive nondecreasing function of x. Letting $n \to \infty$, we define a measure $\mu(a,b)$ as

$$\mu(a,b) = \lim_{n\to\infty} \mu_n(a,b).$$

now we divide the x interval $(0,1)$ into N bins of size $\epsilon = 1/N$, and examine the time asymptotic normalized flux in each bin,

$$p_k = \mu((k-1)\epsilon, k\epsilon), \quad k = 1,2,\ldots .$$

There are different notions of dimensions.[24,26] Here we consider the spectrum D_q of dimensions of the measure μ, where[26]

$$D_q = \lim_{\epsilon\to 0} \frac{1}{q-1}\frac{\ln I_q(\epsilon)}{\ln \epsilon}, \qquad I_q \equiv \sum_{k=1}^{N=1/\epsilon} p_k^q. \tag{B1}$$

For each q value there is a dimension D_q. As an example, if the flux distribution were uniform in x, then $\mu(a,b) = b - a$, $p_k = \epsilon$, $I_q = \epsilon^{q-1}$, and we obtain $D_q = 1$ for all q. As another example, if the flux is all located at a single point (the magnetic field is a delta function in x), then, for some $k = k_0$, $p_{k_0} = 1$, and $p_k = 0$ for all other k; hence $I_q = 1$ and $D_q = 0$.

To calculate D_q for the map (9), we note the following important similarity property: if we imagine that we have a flux p_k in each cell and apply the map to that flux and divide the result by 2, then we obtain N cells of width $\alpha\epsilon$ in $0 \leqslant x \leqslant \alpha$ and N cells of width $\beta\epsilon$ in $\alpha \leqslant x \leqslant 1$, with the α and β intervals each having within it a replica of $\mu(0,x)$ on the whole interval (cf. Refs. 24 and 26 for similar reasoning). Thus to calculate D_q we write I_q as

$$I_q(\epsilon) = I_q^{\alpha}(\epsilon) + I_q^{\beta}(\epsilon),$$

where $I_q^{\alpha}(\epsilon)$ is the sum of the p_k^q over all the cells lying in $0 \leqslant x \leqslant \alpha$ and $I_q^{\beta}(\epsilon)$ is the sum over cells lying in $\alpha \leqslant x \leqslant 1$. From the similarity property we have

$$I_q^{\alpha}(\alpha\epsilon) = \sum_{k=1}^{N=1/\epsilon}\left(\frac{1}{2}p_k\right)^q = \left(\frac{1}{2}\right)^q I_q(\epsilon),$$

$$I_q^{\alpha}(\epsilon) = (1/2^q)I_q(\epsilon/\alpha),$$

and similarly for I_q^{β}. Thus

$$I_q(\epsilon) = 2^{-q}I_q(\epsilon/\alpha) + 2^{-q}I_q(\epsilon/\beta). \tag{B2}$$

As suggested by the definition (B1), we take $I_q(\epsilon) \sim \epsilon^{(q-1)D_q}$. Equation (B2) then yields a transcendental equation for D_q,

$$2^q = \alpha^{-(q-1)D_q} + \beta^{-(q-1)D_q}. \tag{B3}$$

Among the various definitions of the dimensions of a measure, a special role[34] is played by the information dimension, which can be obtained from the limit $q \to 1$ of D_q,

$$D_1 = \lim_{q\to 1} D_q.$$

Taking this limit in Eq. (B3) we have

$$D_1 = (\ln 2)/[\ln(1/\sqrt{\alpha\beta})]; \tag{B4}$$

thus the information dimension of the measure μ, Eq. (B4), is the same as the capacity dimension of the smallest set containing a fraction $\theta < 1$ of the flux, Eq. (17). For a discussion of why this is so see Ref. 24.

The reader familiar with the subject of strange attractors in dissipative dynamics will recognize that the considerations here are very similar to those for strange attractors. It might seem strange that this is so, since the dynamics here is area preserving and the measure generated by typical orbits is uniform in the square, $0 < (x,y) < 1$. Note, however, that here it is the flux that is being attracted to the fractal set (the "strange attractor") rather than the typical orbits, and the measure considered here is the normalized flux.

APPENDIX C: A MORE GENERAL TWO-STRIP MODEL

Here we treat a case that generalizes the result, Eq. (22), which we obtained for the two-strip map Eq. (9). We imagine that the map creates two strips, one of width p and one of width q $(p + q = 1)$, and that the stretching of the p strip is $1/\alpha$ and the stretching of the q strip is $1/\beta$. In the case of Eq. (9), $p = \alpha$ and $q = \beta$. Another case is where we consider the process in Fig. 7 (without the rotation of the third strip) with $\beta = \gamma = \delta \neq \alpha$. In this case, since the β, γ, and δ strips are adjacent and have the same stretching, we consider them as a single merged strip. Thus we have for the p strip $(0 < x < \alpha)$, $p = \alpha$, and, for the (merged) q strip $(\alpha < x < 1)$, $q = 3\beta$. In what follows we do not assume any relationship between the p,q and the α,β. The width of a strip after n iterates is $p^{n-m}q^m$, $m = 0,1,\ldots,n$. The flux in such a strip is $(p/\alpha)^{n-m}(q/\beta)^m$; and (as in Sec. IV C) the number of strips with given n and m is $Z(n,m)$ the binomial coefficient. The total flux in all strips with given n and m is

$$\left(\frac{p}{\alpha}\right)^{n-m}\left(\frac{q}{\beta}\right)^m Z(n,m) = \left[\left(\frac{p}{\alpha}\right) + \left(\frac{q}{\beta}\right)\right]^n p_*^{n-m}q_*^m Z(n,m), \tag{C1}$$

where $p_* = (p/\alpha)/[(p/\alpha) + (q/\beta)]$, and $q_* = (q/\beta)/[(p/\alpha) + (q/\beta)]$. (Note that $p_* + q_* = 1$.) As a function

of m, the quantity $p_*^{n-m}q_*^m Z(n,m)$ is strongly peaked around $m = nq_*$, with a width in m of order $\sqrt{n}$. Thus the total width of strips containing most of the flux is of the order of

$$\sqrt{n}p^{n-m}q^m Z(n,m),$$

evaluated at $m = nq_*$. Using Stirling's approximation

$$p_*^{n-m}q_*^m Z(n,m) = (2\pi n p_* q_*)^{-1/2} \times \exp[-(m-nq_*)^2/2np_*q_*],$$

this gives for the total width of such strips a constant times Q^n, where $Q<1$ (for $\alpha \neq \beta$) and is given by

$$Q = (p/p_*)^{p_*}(q/q_*)^{q_*}.$$

Thus, of the K strips on the surface S, only $k_* \approx KQ^n$ of them will be responsible for most of the numerically computed flux.

For the numerical example on the four-strip baker's map [Eq. (10)] treated in Sec. V B, the strip widths are $\alpha = \frac{1}{3}$ and $\beta = \gamma = \delta = \frac{2}{3}$. In this case we have $p = \frac{1}{3}$ and $q = \frac{2}{3}$, which yield $p_* = \frac{1}{4}$ and $q_* = \frac{3}{4}$. Thus, $Q = 0.9837$, which is very close to unity. The numerical experiment on this map (Fig. 12) runs for $n = 20$ iterates. Since $Q^{20} = 0.72$, we see that $k_* \sim K$ at this time, and therefore the noncanceling flux $\tilde{\Phi}_n$ and the topological entropy should indeed be computed accurately.

The Lyapunov exponent for this general class of maps is

$$\lambda_L = p\ln(1/\alpha) + q\ln(1/\beta). \quad \text{(C2)}$$

From Eq. (6) the growth rate of the flux, or the topological entropy, is

$$\lambda_T = \ln(p/\alpha + q/\beta).$$

Again, it is seen that $\lambda_T \geqslant \lambda_L$ with equality holding only for $\alpha = \beta$.

[1]Ya. B. Zeldovich, A. A. Ruzmaikin, and D. D. Sokoloff, *Magnetic Fields in Astrophysics* (Gordon and Breach, New York, 1984).
[2]E. N. Parker, *Cosmical Magnetic Fields: Their Origin and Activity* (Oxford U.P., Oxford, England, 1979).
[3]H. Alfvén, Tellus **2**, 74 (1950).
[4]S. Childress, J. Math. Phys. **11**, 3063 (1970).
[5]S. I. Vainshtine and Ya. B. Zeldovich, Sov. Phys. Usp. **5**, 159 (1972).
[6]H. K. Moffat, *Magnetic Field Generation in Electrically Conducting Fluids* (Cambridge U.P., Cambridge, England, 1978).
[7]Ya. B. Zeldovich and A. A. Ruzmaikin, Sov. Phys. JETP **51**, 493 (1980).
[8]V. I. Arnold, Ya. B. Zeldovich, A. A. Ruzmaikin, and D. D. Sokolov, Sov. Phys. JETP **81**, 2050 (1981).
[9]V. I. Arnold and E. I. Korkina, Vestn. Mosk. Univ. Mat. Mekh. **3**, 43 (1983) (in Russian).
[10]H. K. Moffat and M. R. E. Proctor, J. Fluid Mech. **154**, 493 (1985). These authors argue that a fast dynamo must have a scale of variation of order $R_m^{-1/2}$
[11]S. A. Molchanov, A. A. Ruzmaikin, and D. D. Sokolov, Sov. Phys. Usp. **28**, 307 (1985).
[12]D. Galloway and U. Frisch, Geophys. Astrophys. Fluid Dyn. **36**, 53 (1986).
[13]H. Strauss, Phys. Rev. Lett. **57**, 2231 (1986).
[14]A. M. Soward, J. Fluid Mech. **180**, 267 (1987). This reference exhibits a steady flow that is nonchaotic and exhibits a fast dynamo. The flow, however, is not smooth. In particular, it has logarithmic singularities in the vorticity at stagnation points.
[15]B. J. Bayly, Phys. Rev. Lett. **57**, 2800 (1986).
[16]B. J. Bayly and S. Childress, Phys. Rev. Lett. **59**, 1573 (1987).
[17]B. B. Kadomtsev, *Plasma Turbulence* (Academic, New York, 1965).
[18]D. Biskamp and R. Chodura, Phys. Rev. Lett. **27**, 1553 (1971).
[19]S. Newhouse, in *Physics of Phase Space*, edited by Y. S. Kim and W. W. Zachary (Springer, Berlin, 1987), p. 2.
[20]B. Mandelbrot, J. Fluid Mech. **62**, 331 (1974).
[21]U. Frisch, P. L. Sulem, and M. Nelkin, J. Fluid Mech. **87**, 719 (1978).
[22]U. Frisch and G. Parisi, in *Turbulence and Predictability in Geophysical Flows and Climate Dynamics*, edited by N. Ghil, R. Benzi, and G. Parisi (North-Holland, New York, 1985), p. 84.
[23]C. Meneveau and K. R. Sreenivasan, Phys. Rev. Lett. **59**, 1424 (1987).
[24]J. D. Farmer, E. Ott, and J. A. Yorke, Physica D **7**, 153 (1983).
[25]S. Newhouse (private communication) uses this in numerical computations of λ_T for dissipative dynamical systems.
[26]H. G. E. Hentschel and I. Procaccia, Physica D **8**, 435 (1983); P. Grassberger, Phys. Lett. A **97**, 227 (1983).
[27]J. M. Greene, in *Long-Time Prediction in Dynamics*, edited by C. Horton, L. Reichl, and A. Szebehely (Wiley, New York, 1983), p. 135.
[28]For nonhyperbolic maps or flows, the approximation in a typical tiny region $w(\mathbf{x}^k) \cong$ const may fail at a small number of the points $\mathbf{x}^k$.
[29]V. I. Arnold, C. R. Acad. Sci. Paris **261**, 17 (1965).
[30]M. Henon, C. R. Acad. Sci. Paris **262**, 312 (1966).
[31]T. Dombre, U. Frisch, J. M. Greene, M. Henon, A. Mehr, and A. M. Soward, J. Fluid Mech. **167**, 353 (1986).
[32]The *ABC* map has been independently studied by M. Feingold, L. P. Kadanoff, and O. Piro (J. Stat. Phys., in press) who were concerned with chaotic convection of a passive scalar.
[33]A short version of our paper has been published [J. M. Finn and E. Ott, Phys. Rev. Lett. **60**, 760 (1988)].
[34]E. Ott, W. D. Withers, and J. A. Yorke, J. Stat. Phys. **36**, 687 (1984).